Initiation of Meiotic Development Is Controlled by Three Post-transcriptional Pathways in *Caenorhabditis elegans*

Ariz Mohammad,* Kara Vanden Broek,† Christopher Wang,† Anahita Daryabeigi,‡ Verena Jantsch,‡ Dave Hansen,† and Tim Schedl*,[1]

*Department of Genetics, School of Medicine, Washington University in St. Louis, Missouri 63110, †Department of Biological Sciences, University of Calgary, T2N 1N4, Canada, and ‡Department of Chromosome Biology, Max F. Perutz Laboratories, University of Vienna, Vienna Biocenter, 1030, Austria

ORCID ID: 0000-0002-1978-682X (V.J.)

ABSTRACT A major event in germline development is the transition from stem/progenitor cells to entry into meiosis and gametogenesis. This transition requires downregulation of mitotic cell cycle activity and upregulation of processes associated with meiosis. We identify the *Caenorhabditis elegans* SCF^{PROM-1} E3 ubiquitin-ligase complex as functioning to downregulate mitotic cell cycle protein levels including cyclin E, WAPL-1, and KNL-2 at meiotic entry and, independently, promoting homologous chromosome pairing as a positive regulator of the CHK-2 kinase. SCF^{PROM-1} is thus a novel regulator of meiotic entry, coordinating downregulation of mitotic cell cycle proteins and promoting homolog pairing. We further show that SCF^{PROM-1} functions redundantly, in parallel to the previously described GLD-1 and GLD-2 meiotic entry pathways, downstream of and inhibited by GLP-1 Notch signaling, which specifies the stem cell fate. Accordingly, *C. elegans* employs three post-transcriptional pathways, SCF^{PROM-1}-mediated protein degradation, GLD-1-mediated translational repression, and GLD-2-mediated translational activation, to control and coordinate the initiation of meiotic development.

KEYWORDS meiotic entry; meiotic development; germline; PROM-1; SCF; GLD-1; GLD-2

A defining feature of the germline is the production of haploid gametes, which unite to form a diploid individual. A key step in germline biology is the transition from mitotically cycling stem/progenitor cells to cells that execute meiotic development and gametogenesis. This transition involves downregulation of gene products that promote mitotic cell cycling and activities and, correspondingly, upregulation of gene products and processes that promote the early steps of meiotic prophase (meiotic entry) and gametogenesis. Meiotic entry includes meiotic S phase and the overt nuclear reorganization processes of homologous chromosome pairing, meiotic chromosome axis and synaptonemal complex assembly, and the initiation of homologous recombination. How control and coordination of the various processes associated with the transition from stem/progenitor cells to meiotic entry and gametogenesis are achieved in animals is only beginning to be understood.

Caenorhabditis elegans is an important model for studying the control of germline development and germline stem cell differentiation. The adult germline is organized as a distal-to-proximal assembly line that displays the process in spatiotemporal order. The distal end of the germline comprises the progenitor zone and leptotene–zygotene, while more proximally are the subsequent stages of meiotic prophase I and gametogenesis (Francis *et al.* 1995a; Dernburg *et al.* 1998; Seidel and Kimble 2015) (Figure 1A). Germ cells move proximally through displacement by mitotic division of more distal cells. The progenitor zone in the adult hermaphrodite extends ~20 "cell diameters" (rows) from the distal end of the germline and contains ~230 germ cells. The current model describes the progenitor zone as consisting of a large

doi: https://doi.org/10.1534/genetics.118.300985
Manuscript received March 29, 2018; accepted for publication June 20, 2018; published Early Online June 25, 2018.
Supplemental material available at Figshare: https://doi.org/10.25386/genetics.6591524.
[1]Corresponding author: Department of Genetics, School of Medicine, Washington University in St. Louis, Campus Box 8232, 4523 Clayton Ave., St. Louis, MO 63110. E-mail: ts@genetics.wustl.edu

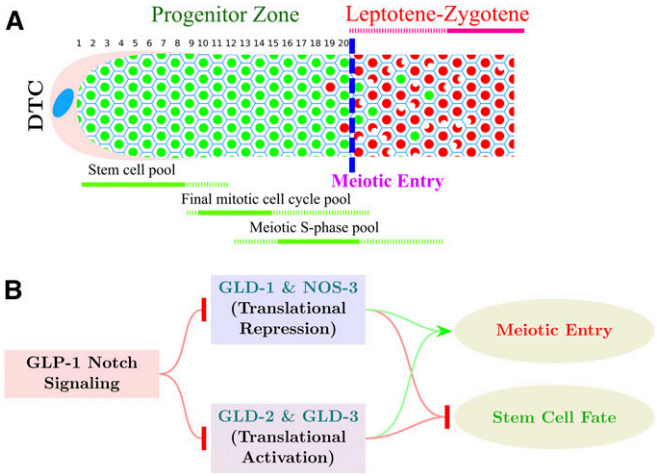

Figure 1 Organization of the distal germline and control of meiotic entry in *C. elegans*. (A) Schematic diagram of the *C. elegans* young-adult hermaphrodite distal germline. Progenitor zone cells are in green; leptotene–zygotene meiotic prophase cells are in red. Blue dashed line indicates operationally defined position of overt meiotic entry. Numbers 1–20 represent distance in cell diameters from the distal tip of the germline to the end of progenitor zone. Extent of the three pools of cells in the progenitor zone is shown in green, below the gonad diagram. (B) Genetic pathway for control of the germline stem cell fate *vs.* meiotic development transition in *C. elegans*. GLP-1 Notch signaling promotes the stem cell fate through inhibition of the redundant GLD-1 and GLD-2 pathways that promote meiotic development.

pool of germline stem cells (~60–80), followed by a pool of cells completing the mitotic cell cycle, and then a more proximal pool of cells in meiotic S phase (Fox and Schedl 2015). Following meiotic S phase is overt meiotic entry where nuclear reorganization, associated with meiotic homolog pairing, and the loading of meiotic chromosomal axes proteins occurs (MacQueen and Villeneuve 2001; Jantsch *et al.* 2007; Jaramillo-Lambert *et al.* 2007; Mlynarczyk-Evans and Villeneuve 2017). In the adult germline, overt meiotic entry can occur in a region extending ~8 cell diameters. This variability in meiotic entry position, at least in part, is a consequence of the asynchronous cycling of the pool of cells completing the mitotic cell cycle and then beginning meiotic S phase, resulting in the different pools of cells partially overlapping in a distal–proximal distribution (Figure 1A; Hansen *et al.* 2004a; Fox *et al.* 2011). Cytological markers that distinguish progenitor zone cells from leptotene–zygotene cells display essentially mutually exclusive accumulation. This permits an operational definition of the position of meiotic entry in the germline as the point where more than half of the cells in a row have switched from one marker to another (Figure 1A, blue dashed line; Figure 2A, Figure 3A and C, Figure 4A,B, Figure 5B, and Figure7, yellow dashed lines in micrographs in *Results*). Cyclin E (CYE-1) is an example of a marker gene product that accumulates in all progenitor zone cells and disappears at meiotic entry (Biedermann *et al.* 2009; Fox *et al.* 2011). Downregulation of mitotic cell cycle activities like CYE-1/CDK-2 following completion of meiotic S phase is likely important for successful meiotic entry; however, the mechanism of downregulation is not well understood. Markers for meiotic entry/leptotene include the phospho-SUN-1 (pSUN-1) nuclear envelope protein and the phosphorylated form of HIM-8 and the three paralogous ZIM autosomal pairing center proteins (pHIM-8/ZIMs), which are essentially absent in the progenitor zone and appear at leptotene. pSUN-1 and pHIM-8/ZIMs are markers for one aspect of meiotic entry, homologous chromosome pairing, and are likely direct substrates of the CHK-2 serine/threonine kinase, a master regulator of homologous chromosome pairing in *C. elegans* (MacQueen and Villeneuve 2001; Oishi *et al.* 2001; Penkner *et al.* 2009; Stamper *et al.* 2013; Kim *et al.* 2015). Restriction of homologous pairing to just after completion of meiotic S phase is important for successful meiotic chromosome segregation, while blocking premature pairing is likely important for efficient mitotic cycling of progenitor zone cells; however, our understanding of the spatial control of homologous pairing at meiotic entry is limited.

GLP-1 Notch receptor signaling promotes the stem cell fate and is activated via Notch ligands expressed by the somatic distal tip cell (DTC), which caps the distal end of the gonad (Hansen and Schedl 2013; Kershner *et al.* 2013). GLP-1 signaling thus generates the distal–proximal polarity of the germline. GLP-1 signaling inhibits two parallel pathways that promote meiotic entry, the GLD-1 and GLD-2 pathways (Figure 1B), through two transcriptional targets, *sygl-1* and *lst-1*, and the FBF Pumilio RNA-binding proteins (Crittenden *et al.* 2002; Kershner and Kimble 2010; Brenner and Schedl 2016; Shin *et al.* 2017). GLD-1 pathway members, GLD-1 and NOS-3, are RNA-binding proteins and are thought to inhibit the translation of gene products required for mitotic cycling and thus promote meiotic entry (Francis *et al.* 1995a; Hansen *et al.* 2004b). The GLD-2 pathway comprises the noncannonical poly-A polymerase, GLD-2, and the Bicaudal-C-type RNA-binding protein, GLD-3, and are thought to promote translation of gene products required for meiotic entry (Figure 1B; Kadyk and Kimble 1998; Wang *et al.* 2002; Eckmann *et al.* 2004). Germ cells proliferate and enter meiosis normally in GLD-1-pathway single mutants and GLD-2-pathway single mutants; however, double mutants with a null allele of either GLD-1-pathway gene together with a null allele of either GLD-2-pathway gene result in a tumorous (overproliferative) germline that occurs through a defect in meiotic entry. Thus, the GLD-1 and GLD-2 pathways function redundantly, in parallel, to promote meiotic entry. GLP-1 signaling is placed genetically upstream and inhibits the GLD-1 and GLD-2 pathways, based on the finding that the overproliferation phenotype of GLD-1 pathway, GLD-2 pathway double mutants are epistatic to the premature meiotic entry phenotype of *glp-1* null (Kadyk and Kimble 1998; Eckmann *et al.* 2004; Hansen *et al.* 2004b).

Genetic experiments indicate that there must be an activity, in addition to the GLD-1 and GLD-2 pathways, that promotes meiotic entry downstream of GLP-1 Notch signaling. First, while *gld-1 gld-2* double null mutants have a tumorous germline, they have some residual meiotic entry which can be

suppressed by a weak temperature-sensitive *glp-1* gain-of-function tumorous allele at the permissive temperature (Hansen *et al.* 2004b). Second, GLP-1 signaling in the distal germline was found to inhibit meiotic entry in distal germ cells, even in the absence of the GLD-1 and GLD-2 pathways (Fox *et al.* 2011).

We previously identified the F-box protein, PROM-1, as well as the SCF E3 ubiquitin-ligase complex proteins, SKR-1/-2 and CUL-1, as genetically functioning in downregulation of CYE-1 levels at meiotic entry (Fox *et al.* 2011). However, these experiments did not determine if CYE-1 is likely a direct substrate for ubiquitin-mediated degradation by SCF employing PROM-1 as a specificity subunit, or whether this SCF complex was more generally involved in downregulation of mitotic gene products at meiotic entry. We also identified PROM-1 as a gene product required for bivalent formation, at least in part, through functioning in homologous chromosome pairing (Jantsch *et al.* 2007). Because PROM-1 has diverse functions associated with meiotic entry and because there are predicted to be factor(s) redundant with the GLD-1 and GLD-2 pathways that promote meiotic entry, we have further explored the function of PROM-1 and its associated SCF complex. We find that CYE-1 and PROM-1 physically interact, that CYE-1 can be polyubiquitinated, and that PROM-1 is conserved at critical residues with other F-box proteins, all suggesting that PROM-1 acts as a specificity subunit for the SCF. We find that SCF^{PROM-1} functions to downregulate multiple mitotic cell cycle proteins at meiotic entry and, independently, SCF^{PROM-1} promotes homologous chromosome pairing as a positive regulator of CHK-2. Finally, we provide evidence that SCF^{PROM-1} acts redundantly, in parallel, with the GLD-1 and GLD-2 pathways to coordinate meiotic entry in the hermaphrodite and male germlines.

Materials and Methods

Strain maintenance and synchronization

All the strains were maintained at 20°, unless otherwise stated. All gene mutations employed, with the exception of *fem-3*(*q20*), are the canonical null allele (http://WormBase.org). *Cis*-recombinants were made using standard methods (Fay 2013). Sterile or lethal alleles were maintained over genetic balancers; the full genotype of the strains used in this study is found in Supplemental Material, Table S1. In this study, the "young-adult" stage employed in the analysis is 8 hr after the L4/adult molt; this slightly younger stage than the typical 1-day after mid-L4 was used because overproliferation phenotypes were more straightforward to analyze and quantify due to fewer cells and reduced potential secondary effects of the large proximal overproliferation in tumorous animals such as *gld-1* null. To obtain synchronized populations, adult hermaphrodites were bleached, allowed to hatch overnight in S-medium, and synchronized L1 worms were provided food and grown at the desired temperature. After 46 hr at 20°, L4-adult molting worms were picked to a separate plate and were used for dissection after 8 hr.

Immunohistochemistry

Gonads (germlines) were dissected and stained using the batch method as described (Fox *et al.* 2011). Briefly, worms of the desired genotype were dissected in PBS with Tween 20 (PBST) buffer (150 mM NaCl, 3 mM KCl, 2 mM KH_2PO_4, 8 mM Na_2HPO_4, 0.1% Tween 20, pH 7.4) with 0.2 mM levamisole. For most of the antibodies used, dissected gonads were fixed in a 3% paraformaldehyde (PFA) solution (3% PFA, 0.1 M K_2HPO_4, pH 7.2) for 10 min and postfixed in −20° prechilled methanol for 10 min. Fixed gonads, after three 10-min washes with PBST, were blocked with 30% goat serum for 30 min and then incubated with the desired primary antibodies diluted in 30% goat serum at 4° overnight. For KNL-2 and REC-8 (rat) staining, after 3% PFA fixation, gonads were postfixed in −20° prechilled methanol for 1 hr. For DSB-1 and COH-3/4 antibody staining, the 3% PFA fixation time was increased to 30 min. For pHIM-8/ZIMs and HIM-8, incubation time with primary antibody was 2 hr at room temperature. In all cases, gonads were then washed three times with PBST and incubated with desired secondary antibodies, diluted in 30% goat serum, at 4° overnight. The germlines, after two 10-min washes with PBST, were incubated with 0.1 g/ml DAPI in PBST for 10 min. The germlines were then suspended in a drop of antifading agent (DABCO or Vectashield) and spread over an agarose pad on a microscope slide.

To visualize REC-8 on meiotic chromosomes (Figure 10A), adult hermaphrodites were dissected in PBST and the gonads that adhered to slides were fixed in 1% PFA for 5 min (Martinez-Perez and Villeneuve 2005). For immunostaining, the gonads were blocked in 3% BSA in PBST for 20 min and incubated with primary REC-8 antibody (dilution: 1:10,000; #2947002, Novus biological) overnight at 4°. Immunostaining was followed by incubation with the secondary antibody (anti-rabbit; dilution 1:500; #A11034, Invitrogen, Carlsbad, CA) for 2 hr at room temperature.

Antibodies that were used in these studies: CYE-1 (mouse, 1:100) (Brodigan *et al.* 2003), REC-8 (rat, 1:100) (Pasierbek *et al.* 2001), REC-8 (rabbit, 1:100; Novus Biological), GLD-1 (rabbit, 1:100) (Jones *et al.* 1996), KNL-2 (rabbit, 1:100) (Maddox *et al.* 2007), HIM-8 (guinea pig, 1:100) (Phillips *et al.* 2005), GFP (rabbit, 1:200; a gift from S. Arur, MD Anderson Cancer Center), HIM-3 (rabbit, 1:100) (Zetka *et al.* 1999), pHIM-8/ZIMs (rabbit, 1:100) (Kim *et al.* 2015), pSUN-1 (pS8; guinea pig, 1:700) (Penkner *et al.* 2009), WAPL-1 (rabbit, 1:2000; Novus Biological), COH-3/4 (rabbit, 1:100) (Severson and Meyer 2014), DSB-1 (guinea pig, 1:100) (Stamper *et al.* 2013), phospho-CDC-6 (pCDC-6) (rabbit, 1:100) (Kim and Kipreos 2007), phospho-(Ser10)-Histone 3 (pH3) (rabbit, 1:500; Upstate), nuclear lamin (GP28, guinea pig, 1:2000) (Liu *et al.* 2000), MSP (mouse, 1:10,000) (Kosinski *et al.* 2005), PGL-1/-3 [KT3-s, 1:10; Developmental Studies Hybridoma Bank (DSHB), University of Iowa].

Images were captured using a spinning disk confocal microscope (PerkinElmer-Cetus, Norwalk, CT). The images

were stitched together using either Volocity software (PerkinElmer) or Stitching plugin in Fiji (Preibisch *et al.* 2009; Schindelin *et al.* 2012) and were further assembled using Fiji and Inkscape.

Cell diameters, nuclei counts, and position of meiotic entry

The length of the gonadal region of interest was calculated using either Volocity software or the "cell counter" plugin in Fiji. Distance, in cell diameter, is the number of rows of nuclei starting from the distal tip of the gonad and is calculated as described (Hubbard 2007) (Figure 1A). Nuclei counts were performed using Fiji and a modified R script, as described (Seidel and Kimble 2015), to remove double counting wherever required. All the data were stored in SQLiteStudio (SQLite3 database) and were further analyzed using RStudio/R programming language.

Graphs were plotted using the ggplot2 package in R programming language (http://ggplot2.org). Statistical significance was determined using either two-tailed Student's *t*-test (for $n < 30$) or *Z*-test (for $n \geq 30$). The significance bars were generated using the ggsignif package (https://CRAN.R-project.org/package=ggsignif) and with custom R scripts, which can be made available upon request. Diagrams in Figure 1 and Figure 11 are generated using the PGF/TikZ package in LaTeX (https://ctan.org/pkg/pgf?lang=en).

Determination of the position of meiotic entry shown in the figures depends on the genotype and primary antibodies employed. In genotypes where the transition from the progenitor zone to meiotic entry is largely normal, it is the point where more than half of the cells in a row have switched from staining for a progenitor zone marker to a meiotic prophase marker. In genotypes containing SCF^{PROM-1} loss of function, it is the point where more than half of the cells in a row have switched to HIM-3- or COH-3/4-positive nuclei in costaining experiments or, in cases where another rabbit primary antibody was used in place of anti-HIM-3 or anti-COH-3/4 (*e.g.*, anti-pHIM-8/ZIMs; Figure 3C), the average position was determined in separate experiments staining for HIM-3 or COH-3/4 in the same genotype under identical conditions.

RNA-interference experiments

RNA interference (RNAi) by bacterial feeding experiments for *cul-1* and *skr-1* were performed using the clones described in Nayak *et al.* (2002). Overnight-grown bacteria cultures carrying the desired clone were used to seed NGM plates containing 1 mM IPTG and 100 μg/ml ampicillin (RNAi plates). AMJ345 (*jamSi2 II*; *rde-1*(*ne219*) *V*; Marré *et al.* 2016) was used for largely germline-restricted RNAi. L4 worms were placed on RNAi plates and allowed to grow/lay eggs at 20° for 24 hr. For *cul-1* RNAi, mothers were picked off plates and, ~60 hr later, adults were picked, dissected, and stained. *cul-1* RNAi results in pleiotropic phenotypes from embryonic lethality to worms arrested at various larval stages, along with fully grown sterile and fertile adults. Sterile animals were analyzed, which included a large number of germlines with mitotic cell cycle arrest, as well as a smaller number with meiotic prophase defects including delayed pairing. Germlines lacking mitotic cell cycle arrest were used in this study and thus represent partial *cul-1* messenger RNA (mRNA) knockdown. For *cul-1* RNAi on *gld-1* worms, which are sterile by themselves, >100 animals were picked for 5-ethynyl-2′-deoxyuridine (EdU) labeling/dissection and staining. For *skr-1* RNAi, worms were bleached after 24 hr of RNAi and allowed to hatch overnight in S-medium. The synchronized L1s were plated on freshly made RNAi plates. Larvae were picked after 26 hr posthatch for early L3. *cye-1* RNAi was performed as previously described (Fox *et al.* 2011).

EdU-labeling experiments

EdU-labeling experiments were performed by feeding worms on EdU-labeled bacteria as described (Fox *et al.* 2011). Since >99% of nuclei in the progenitor zone incorporate EdU in about ~3.5 hr of continuous EdU labeling (Fox *et al.* 2011), unless otherwise noted, all the EdU-labeling experiments were performed with 4-hr, EdU-labeled bacteria feeding. For EdU labeling of young adults, synchronized 4-hr, post-L4/adult molt worms were washed off OP50 plates and placed on EdU plates. After 4 hr of feeding, they were washed off, dissected, and stained. After primary and secondary antibody staining, gonads were treated with the EdU-detection reaction using an EdU-labeling kit (Invitrogen) followed by DAPI staining. For early L3, larvae were picked after 26-hr posthatch and fed on EdU-labeled plates for 30 min before dissection. Because there are mitotic cycling cells in both the germline and somatic gonad in L3 worms, dissected gonads were costained with anti-PGL-1/-3 antibody to specifically mark and identify germ cells.

Ubiquitination assay

Full-length complementary DNA (cDNA) of *prom-1* was subcloned into *pcDNA3.1B-Myc-His* at *Kpn*I and *Not*I sites using oligos E18 and E19 (pDH384). A full-length cDNA of *cye-1* was subcloned into *pCMV-Tag2-FLAG* using *Bam*HI and *Xho*I restriction sites using oligos E20 and E21 (pDH382). The vectors, including *pCMV-HA*::*Ubiquitin*, were gifts from E. Kipreos (University of Georgia, Athens). The sequences of the oligos used are as follows:

E18: GGG GGT ACC ATG GAT AAA TCA ACA
E19: TTT GCG GCC GCA CAG TAG TTT CAT
E20: AAA GGA TCC ATG GCT GGA AGA AAG
E21: CCC CTC GAG TTA GAA AAG TCG TTG

HEK293T cells were transiently transfected with combinations of the following vectors: (1) *pCMV-Tag2-FLAG-CYE-1* and *pcDNA3.1B-Myc-His-PROM-1*, (2) *pcDNA3.1B-Myc-His-PROM-1* and *pCMV-HA*::*Ubiquitin*, (3) *pCMV-Tag2-FLAG-CYE-1* and *pCMV-HA*::*Ubiquitin*, or (4) *pCMV-Tag2-FLAG-CYE-1*, *pcDNA3.1B-Myc-His-PROM-1*, and *pCMV-HA*::*Ubiquitin*. Cotransfection into HEK293T cells was performed using 60 μl of linear polyethyleneimine MW25K (PolyScience, Warrington, PA) (1 mg/ml in H_2O, neutralize with HCl to pH 7.2) and

up to 15 μg of the total DNA in 1.5 ml Dulbecco's modified Eagle's medium (DMEM) plus L-glutamine (free of serum and antibiotic). This mixture was then added to 60–80% confluent HEK293T cells grown in a 100-mm culture dish containing 5 ml DMEM plus L-glutamine and incubated for 40 min (37° and 5% CO_2). DMEM plus L-glutamine and (antibiotic-free) fetal bovine serum (5 ml) was then added and left overnight (37° and 5% CO_2). The media were refreshed after 24 hr. At 40 hr after transfection, cells were washed three times with ice-cold PBS and homogenized using a Dounce homogenizer in lysis buffer (20 mM HEPES, pH 7.2, 200 mM NaCl, 6 mM $MgCl_2$, 2 mM EGTA, 0.6 M sucrose, and 1% Triton X-100) with a Protease Inhibitor Cocktail (Roche).

Immunoprecipitation was performed using anti-FLAG antibodies (Sigma Chemical, St. Louis, MO). Briefly, anti-FLAG antibodies were coupled to Protein G Sepharose beads (Sigma Chemical), as previously described (Polanowska *et al.* 2004), at a concentration of 12 μg per 100 μl beads. Each immunoprecipitation was performed by incubating 1 mg of protein extract with 25 μl of beads overnight at 4°. The protein samples were washed four times with lysis buffer plus the Protease Inhibitor Cocktail and dissolved in 5× SDS-PAGE loading buffer for Western blot analysis.

Proteins were resolved on a 10% SDS-PAGE gel and transferred to a 0.45 μm BioTrace polyvinylidene fluoride membrane (Life Sciences) using Mini-Trans Blot Cell (Bio-Rad, Hercules, CA). The membrane was subsequently denatured for 30 min at 4° in denaturing solution (6 M guanidine HCL, 20 mM Tris, pH 7.4, 1 mM PMSF, 5 μM β-mercaptoethanol) as previously described (Penengo *et al.* 2006) and blocked in 5% Carnation milk in 1× TBS. The membrane was then probed with rat anti-HA antibodies (Roche) at 1:1000 dilution and rabbit anti-FLAG antibodies at 1:500 dilution (Thermo Scientific). Crude protein extracts were also resolved and denatured, as described above, and then probed with mouse anti-MYC antibodies (9E10, Hybridoma cell line from DSHB) and rabbit anti-actin antibodies at 1:3000 dilution (Sigma Chemical). Signals were visualized using Amersham ECL Select Detection Reagent (GE Healthcare) and exposed to Carestream Kodak Biomax MR film (VWR).

Yeast two-hybrid system

Full-length cDNA of *prom-1* was subcloned into pGBKT7 [containing the GAL4 DNA-binding domain fusion (BD) and tryptophan reporter gene] and pGADT7 [containing the GAL4 activation domain fusion (AD) and leucine reporter gene], from the Matchmaker Two-Hybrid System 3 (Clontech), at *Nde*I and *Xma*I restriction sites using oligos HA20 and HA26. Full-length cDNA of *cye-1* was subcloned into pGBKT7 (BD) and pGADT7 (AD) at *Bam*HI and *EcoR*I restriction sites using oligos HA22 and HA23. Combinations of pDH468 (*prom-1* in pGADT7), pDH472 (*prom-1* in pGBKT7), pDH455 (*cye-1* in pGADT7), pDH456 (*cye-1* in pGBKT7), and empty vector controls were cotransformed into the *Saccharomyces cerevisiae* strain AH109 Matchmaker yeast strain (Matchmaker Two-Hybrid System 3). Cotransformation was tested on tryptophan- leucine-deficient selective medium. Interaction in the two-hybrid system was tested on histidine-deficient (medium stringency) and histidine- and adenine-deficient selective media (high stringency). The sequences of the oligos are as follows:

HA20: CGC TCA TAT GAT GGA TAA ATC AAC ACC CAG GCG G
HA22: CCA GTG AAT TCA TGG CTG GAA GAA AGT C
HA23: CGA TGG ATC CCT TAG AAA AGT CGT TGC GG
HA26: TTA CAC CCG GGT TAC AGT AGT TTC ATC AAT ACC GGC

Data availability

The data required for the results presented in the article are present in the figures, supplementary figures, figure legends, tables, and the article body. Table S1 provides a complete list of all the strains used for this study. All strains and reagents used are available upon request. Supplemental material available at Figshare: https://doi.org/10.25386/genetics.6591524.

Results

PROM-1 targets CYE-1 for ubiquitin-mediated degradation

CYE-1 accumulates in the progenitor zone of the *C. elegans* hermaphrodite germline, disappears at meiotic entry, and reappears in late pachytene nuclei (Brodigan *et al.* 2003; Fox *et al.* 2011). Putative components of an SCF E3 ubiquitin ligase, including CUL-1, a Cullin homolog (Kipreos *et al.* 1996); SKR-1/-2, Skp homologs (Nayak *et al.* 2002); and PROM-1, an F-box protein (Jantsch *et al.* 2007), are required for downregulation of CYE-1 upon entry into meiotic prophase (Fox *et al.* 2011). GLD-1, a translational repressor (Francis *et al.* 1995a; Lee and Schedl 2010), is not required for downregulation of CYE-1 at meiotic entry, but keeps CYE-1 levels low in the pachytene region (Biedermann *et al.* 2009; Fox *et al.* 2011). We first confirmed and quantified the distal–proximal extent of failure to downregulate CYE-1 at meiotic entry in *prom-1* null mutant, young-adult, hermaphrodite germlines. In wild-type germlines, CYE-1 accumulation extends 21 cell diameters from the distal tip (DT) of the germline, while in *prom-1* mutants it extends 38 cell diameters (Figure 2, A and B). Further, CYE-1 ectopically accumulates in *skr-1/-2* RNAi germlines where *skr-1* or *skr-2* single RNAi gives an identical phenotype, likely because of cross-RNAi (Nayak *et al.* 2002; Fox *et al.* 2011). We used genetic mutants to examine which of these two genes is responsible for CYE-1 downregulation at entry into meiotic prophase. Only *skr-2* null mutant germlines show ectopic CYE-1, suggesting that SKR-2 plays a major role in downregulation of CYE-1 in young adults (Figure 2B, also see below). A strong *cul-1* loss-of-function mutation results in L3 or L4 larval arrest (Kipreos *et al.* 1996); therefore, we used partial *cul-1* RNAi knockdown in a genetic background that is largely refractory

to somatic RNAi, employing a strain containing a knockout of the essential RNAi factor *rde-1* and expressing *rde-1*(+) in the germline using the *mex-5* promoter (Marré *et al.* 2016; *Materials and Methods*). We observed modest but statistically significant ectopic accumulation of CYE-1 in *cul-1* RNAi germlines (Figure 2B). Thus, in genetic tests, *prom-1*, *skr-2*, and *cul-1* behave similarly in downregulation of CYE-1 at meiotic entry.

PROM-1 is homologous to human F-box protein FBXO47, with sequence conservation across the full length of the protein, and contains an F-box motif based on conservation of residues most highly conserved in canonical F-box proteins (Figure S1); therefore, PROM-1 likely functions as an F-box protein. Our analysis of CYE-1 downregulation above suggests that PROM-1 could act as a specificity subunit in an SCF complex with SKR-1/-2 and CUL-1 to mediate ubiquitination of CYE-1 at the leptotene–zygotene stage in the germline, leading to its degradation in the wild-type animals. To determine if PROM-1 could be the specificity subunit in an SCF complex targeting CYE-1, we tested if PROM-1 and CYE-1 physically interact using a yeast two-hybrid assay. We found that PROM-1 and CYE-1 interact in this assay (Figure S2), consistent with PROM-1 functioning as a specificity subunit targeting CYE-1 for degradation. To test if CYE-1 can be polyubiquitinated for degradation, a mammalian tissue culture cell ubiquitination assay was performed (Kim and Kipreos 2007). PROM-1 (tagged with MYC) and CYE-1 (tagged with FLAG) were subcloned into expression vectors and transfected into HEK293T cells (*Materials and Methods*; Figure 2C). This assay is based on the assumption that the mammalian orthologs of the E3 ubiquitin-ligase complex SKR, CUL-1, *etc*., will interact with *C. elegans* PROM-1, an F-box protein that will then provide substrate specificity for the complex. Ubiquitin is then added to an F-box protein-bound substrate protein by the action of an E3 ubiquitin ligase, and further ubiquitination of the substrate results in various polyubiquitinated products, producing a smear on an SDS polyacrylamide gel. Polyubiquitination of CYE-1 (smear) was observed when PROM-1 was present, demonstrating the CYE-1 can be a target of ubiquitination. Significant polyubiquitination also occurs in the absence of PROM-1, suggesting that an endogenous mammalian protein is capable of providing specificity to the SCF complex. Indeed, FBXO47 (the mammalian homolog of PROM-1) is expressed in HEK293T cells (Hruz *et al.* 2008). Together, the above results indicate that PROM-1 is an F-box protein that directly targets CYE-1 for ubiquitin-mediated degradation at meiotic entry. The genetic analysis described below shows that PROM-1, SKR-1/-2, and CUL-1 have essentially identical functions in pairing, downregulation of other mitotic cell cycle factors at meiotic entry, and interactions with the GLD-1 and GLD-2 pathways, consistent with them acting together as an SCF complex. Hereafter, we use SCF^{PROM-1} to indicate the E3 ubiquitin ligase comprising PROM-1, CUL-1, and SKR-1/-2, which together act to control various germline processes necessary for meiotic entry.

Meiotic entry occurs in SCF^{PROM-1} loss-of-function germlines

prom-1 mutant germlines lack a typical leptotene–zygotene zone but rather display an "extended early leptotene region" (Zickler and Kleckner 1998; Jantsch *et al.* 2007). Given the absence of the polarized/crescent-shaped DNA nuclear morphology associated with meiotic entry, as well as ectopic CYE-1 accumulation in the extended early leptotene region in SCF^{PROM-1} loss-of-function germlines, we sought alternative markers to quantitatively assess the position where germ cells enter meiosis and the distal–proximal distribution of mitotically cycling cells. We found that the accumulation of the meiotic chromosome axis protein HIM-3 in *prom-1* and *skr-2* mutant germlines was similar in position to wild type, indicating that the cells ectopically expressing CYE-1 had entered into meiosis (Figure S3A; Jantsch *et al.* 2007). Likewise, meiotic cohesion proteins COH-3/COH-4 (Severson and Meyer 2014), which appear at meiotic entry in wild-type germlines, had a similar accumulation pattern in *prom-1* mutant germlines (Figure S3B). Additionally, GLD-1 accumulated in a similar pattern in wild type and *prom-1* young-adult mutant hermaphrodites, rising ~20-fold in a sigmoidal-like pattern from the distal end (Brenner and Schedl 2016; Figure S3C).

Since markers used to define the progenitor zone, such as CYE-1 and nucleoplasmic REC-8 (see below), accumulate ectopically in SCF^{PROM-1} mutant germlines, they cannot be used as markers to determine if there are ectopic mitotic cycling cells. Instead, we used EdU to identify cells undergoing S phase (Salic and Mitchison 2008; Fox *et al.* 2011). Hermaphrodites were fed EdU-labeled bacteria for 4 hr and then immediately dissected and stained for analysis (*Materials and Methods*). In wild-type animals, 4-hr EdU labeling results in essentially all cells in the progenitor zone being labeled, as well as some leptotene–zygotene cells that transitioned from meiotic S phase during the labeling period (Fox *et al.* 2011). From the labeling, we define a region (in cell diameters from the DT), which contains only EdU positive (+) germ cells, as the "continuous EdU zone" (Figure S3, D and E). The continuous EdU zone length in *prom-1* and *skr-2* mutants was indistinguishable from the wild-type length (~25 cell diameters) (Figure S3, D and E), which is consistent with a previous qualitative assessment of S-phase position from Cy3-dUTP labeling in *prom-1* mutants (Jantsch *et al.* 2007). Taken together, these results indicate that despite the extended early leptotene region and ectopic CYE-1 accumulation, the position of the switch to meiotic entry in SCF^{PROM-1} mutant germlines remains similar to wild type.

CHK-2-dependent homologous chromosome pairing fails to occur at meiotic entry in SCF^{PROM-1} loss of function

prom-1 mutants are partially defective in homologous chromosome pairing and double-strand-break (DSB) processing (Jantsch *et al.* 2007). Nayak *et al.* (2002) found that *skr-1/-2* RNAi germlines contain univalent diakinetic chromosomes,

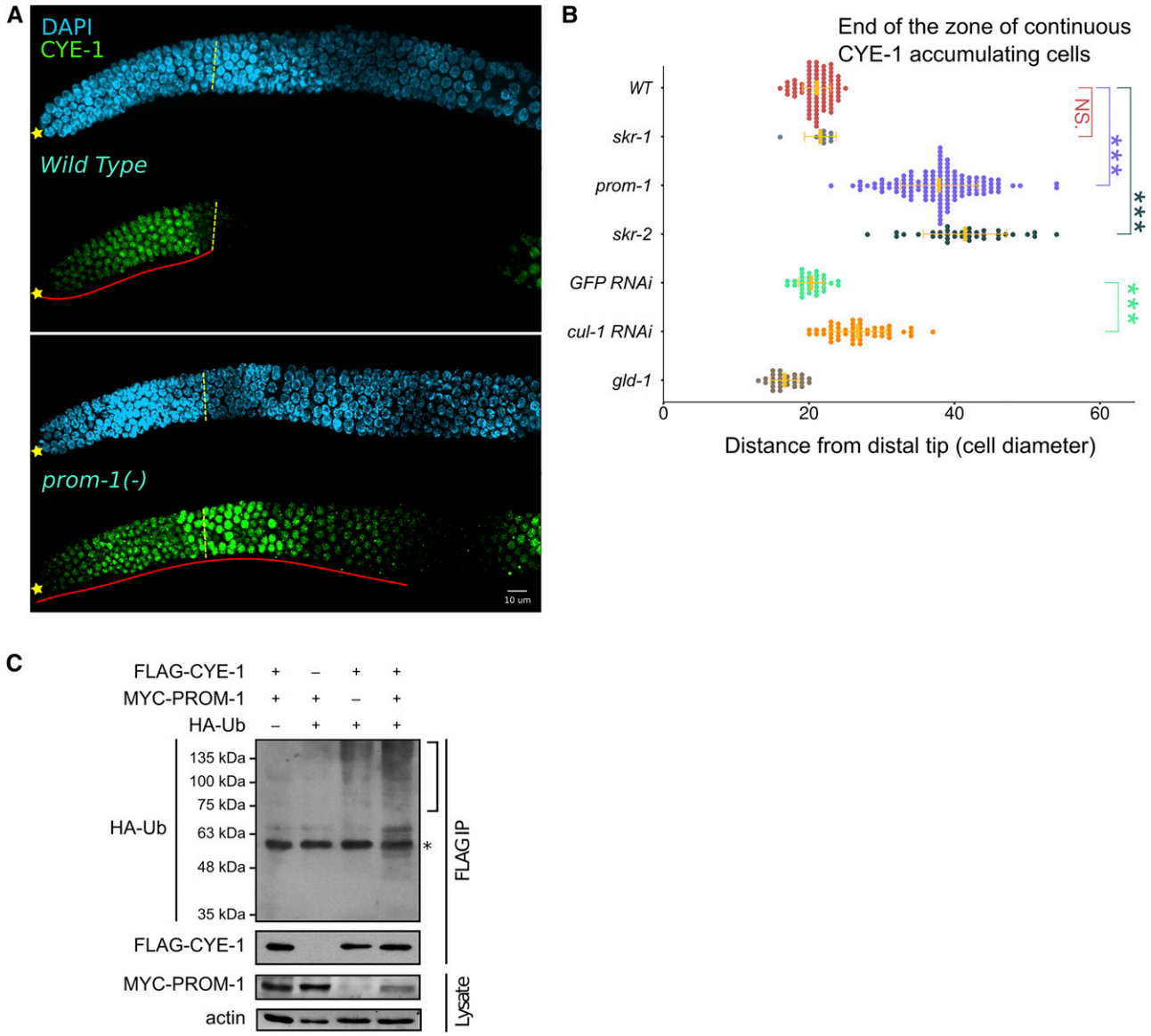

Figure 2 SCF^{PROM-1} is required for downregulation of CYE-1 at meiotic entry. (A) Images of CYE-1-stained (green) distal wild-type (top) or *prom-1* mutant (bottom) germlines from dissected young adult hermaphrodites, costained with DAPI (cyan). ☆'s indicate distal gonadal end. Dashed yellow lines indicate position of overt meiotic entry; see *Materials and Methods* for how the position of overt meiotic entry was determined here and in other figures. Solid red lines highlight the zone of continuous CYE-1 accumulation. (B) Graph showing distance, in cell diameters, between the DT of the germline and the row of cells at proximal end of the continuous zone of CYE-1 staining [solid red line in (A)] for young-adult hermaphrodites of indicated genotype. *cul-1* RNAi, here and in other figures, was performed in worms of the genotype *jamSi2*[*mex-5p*::*rde-1*(+)] *II*; *rde-1*(*ne219*) *V* to largely restrict RNAi knockdown to the germline. Data are plotted as horizontal dot plots with each dot representing length in cell diameter to zone end for one gonad. Thick vertical lines represent mean and horizontal lines represent mean ± SD. *P*-value ≤ 0.01 (*); ≤ 0.001 (**); ≤ 0.0001 (***); > 0.01 non-significant (NS.). (C) Different combinations of *C. elegans* FLAG-CYE-1, MYC-PROM-1, and HA-ubiquitin (HA-UB) constructs were transiently expressed in HEK293T cells, followed by FLAG-CYE-1 immunoprecipitation (IP). The immunoprecipitants were analyzed by Western blot with anti-HA and anti-FLAG antibodies. Slower migrating polyubiquitinated forms of CYE-1 are slightly increased in the presence of PROM-1 (see text). The expression of MYC-PROM-1 was analyzed in whole cell lysates. The bracket marks polyubiquitination of CYE-1. * represents cross-reactivity between the mouse anti-FLAG antibody used for IP and the rat anti-HA antibody. WT, wild type.

which could also be due to a failure in pairing. We first asked if a pairing defect is also observed in *skr-2* and *cul-1* loss-of-function germlines.

HIM-8 specifically binds to the X-chromosome pairing center; in wild type, HIM-8 is visible as two foci in progenitor zone nuclei, but at the transition to leptotene–zygotene these foci start to merge and by early pachytene they appear as a single bright focus or a closely spaced doublet in all the nuclei (Phillips *et al.* 2005). We confirmed the Jantsch *et al.* (2007) result that X-chromosome pairing is absent in the 20 cell diameters just proximal to the progenitor zone, the extended early leptotene region, in *prom-1* mutant germlines (Figure

S4A). We found that *skr-2* mutant and *cul-1* RNAi (unpublished result) germlines also showed absence of X-chromosomal pairing in the extended early leptotene region. Thus, *prom-1* mutants and loss of its partners, *skr-2* and *cul-1*, show a similar X-chromosome pairing defect. Although X-chromosome pairing is absent in the extended early leptotene region in SCF^{PROM-1} loss-of-function germlines, by pachytene some level of paired HIM-8 foci was observed (Figure S4A; unpublished results).

The CHK-2 kinase is a master regulator promoting meiotic homologous chromosome pairing in *C. elegans* (MacQueen and Villeneuve 2001; Oishi *et al.* 2001; Stamper *et al.* 2013; Kim *et al.* 2015). The SCF^{PROM-1} loss-of-function HIM-8 pairing defect could reflect SCF^{PROM-1} acting as a positive regulator of CHK-2, controlling multiple aspects of pairing, or reflect SCF^{PROM-1} functioning in only a subset of pairing-associated activities. To examine if SCF^{PROM-1} loss of function alters CHK-2 activity, we assessed the phosphorylation status of two sets of likely direct substrates, SUN-1 and HIM-8/ZIMs, using phospho-specific antibody staining. pSUN-1 (phosphorylated on Ser8) appears on the nuclear envelope at the boundary of the progenitor zone and leptotene–zygotene region in wild type (Penkner *et al.* 2009). However, in *prom-1*, *skr-2*, and *cul-1* loss-of-function germlines, pSUN-1 was absent in the extended early leptotene region and, similar to paired HIM-8 foci, eventually accumulates in pachytene (Figure 3, A and B). The CHK-2 pHIM-8/ZIMs are required for pairing and appear as foci at the boundary of the progenitor zone and leptotene–zygotene region in wild type (Kim *et al.* 2015). We found that pHIM-8/ZIMs foci were absent in the extended early leptotene region of SCF^{PROM-1} loss-of-function germlines (Figure 3, C and D). The absence of phosphorylation of HIM-8/ZIMs and SUN-1 (S8), both likely direct substrates of CHK-2, indicates that CHK-2 is not active in the extended early leptotene region of SCF^{PROM-1} loss-of-function germlines.

To obtain further support that CHK-2 activity is absent from the extended early leptotene region of *prom-1* mutants, we analyzed two proteins, DSB-1 and dynein heavy chain 1 (DHC-1), whose localization is dependent on CHK-2 activity. DSB-1, which is required for DSB formation, localizes to chromatin of nuclei at meiotic entry in a CHK-2-dependent manner, although independent of DSB formation (Stamper *et al.* 2013). If CHK-2 activity is absent in the extended early leptotene region, we predict that DBS-1 would fail to accumulate in SCF^{PROM-1} mutant germlines. Consistent with this, we found that DSB-1 was reduced/absent from chromatin in the extended early leptotene region of *prom-1* mutant germlines (Figure S4B). DHC-1 promotes chromosome movement for pairing and, in wild type, appears as aggregates on the surface of the nuclear envelope at leptotene–zygotene in a CHK-2-dependent manner (Sato *et al.* 2009). In *prom-1* mutant germlines, DHC-1 aggregates at the nuclear envelope were absent in the extended early leptotene region and, similar to pSUN-1 and pHIM-8/ZIMs, eventually appeared in pachytene (Figure S4C). Together, the failure of CHK-2-dependent accumulation of pSUN-1, pHIM-8/ZIMs, DSB-1, and DHC-1 at the extended early leptotene region in SCF^{PROM-1} loss-of-function germlines supports the conclusion that SCF^{PROM-1} is a positive regulator of CHK-2 activity.

CHK-2 activity and CYE-1 levels at meiotic entry appear to be independently controlled

As described above, CHK-2 activity appears abruptly at meiotic entry (Kim *et al.* 2015), which coincides with downregulation of CYE-1. Intriguingly, in SCF^{PROM-1} loss-of-function germlines where CHK-2 activity is absent at meiotic entry, the location where CHK-2 activity appears to be eventually restored roughly coincides with where downregulation of ectopic CYE-1 finally occurs (Figure 2, A and B, and Figure 3). This raises the possibility that CYE-1 could be an inhibitor of CHK-2 activity in the progenitor zone and ectopic CYE-1–CDK-2 could cause the delayed CHK-2 activity observed in SCF^{PROM-1} mutant germlines. However, a separation-of-function result from *cul-1* RNAi suggests that the absence of CHK-2 activity at meiotic entry in SCF^{PROM-1} loss of function is unlikely to be due to ectopic CYE-1. The extension of CYE-1 accumulation was only modestly increased in *cul-1* RNAi germlines as compared to the more dramatic extension in *prom-1* mutant germlines. In contrast, pSUN-1 staining and pHIM-8/ZIMs foci, readouts of CHK-2 activity, were robustly delayed following *cul-1* RNAi, similar to *prom-1* mutant germlines (Figure S5, A and B; note the gap between the end of CYE-1 and the start of pHIM-8/ZIM staining). Furthermore, if ectopic CYE-1 repressed CHK-2 activity, then loss of CYE-1 is predicted to result in increased CHK-2 activity and pairing. However, following *cye-1* RNAi in *prom-1* mutants starting at the L4 stage and examination 42 and 66 hr later, while CYE-1 levels were reduced or absent, accumulation of pSUN-1 was still delayed relative to meiotic entry, as assessed by HIM-3 staining (Figure S5C; unpublished results). Additionally, CYE-1 was downregulated at meiotic entry in pairing-defective *him-19* mutant germlines, but CHK-2-dependent pSUN-1 failed to appear until late pachytene (unpublished results). These observations indicate that the absence of CHK-2 activity at meiotic entry in SCF^{PROM-1} mutant germlines is not due to ectopic CYE-1.

We also considered the possibility that loss of CHK-2 activity and/or the pairing defect in SCF^{PROM-1} loss-of-function germlines could be responsible for ectopic accumulation of CYE-1 in the extended leptotene region. We examined CYE-1 accumulation in pairing-defective *chk-2*, *plk-2*, and *him-19* null mutants (Penkner *et al.* 2009; Tang *et al.* 2010). We observed that CYE-1 is downregulated in all three mutants at the position where the transition to leptotene occurs in wild type (unpublished results). Thus, downregulation of CYE-1 at meiotic entry does not require the kinases CHK-2 or PLK-2, HIM-19, or pairing *per se*.

SCF^{PROM-1} is required for downregulation of mitotic cell cycle regulators at meiotic entry

Since SCF^{PROM-1} functions in downregulation of CYE-1 at meiotic entry, we asked if SCF^{PROM-1} downregulates other

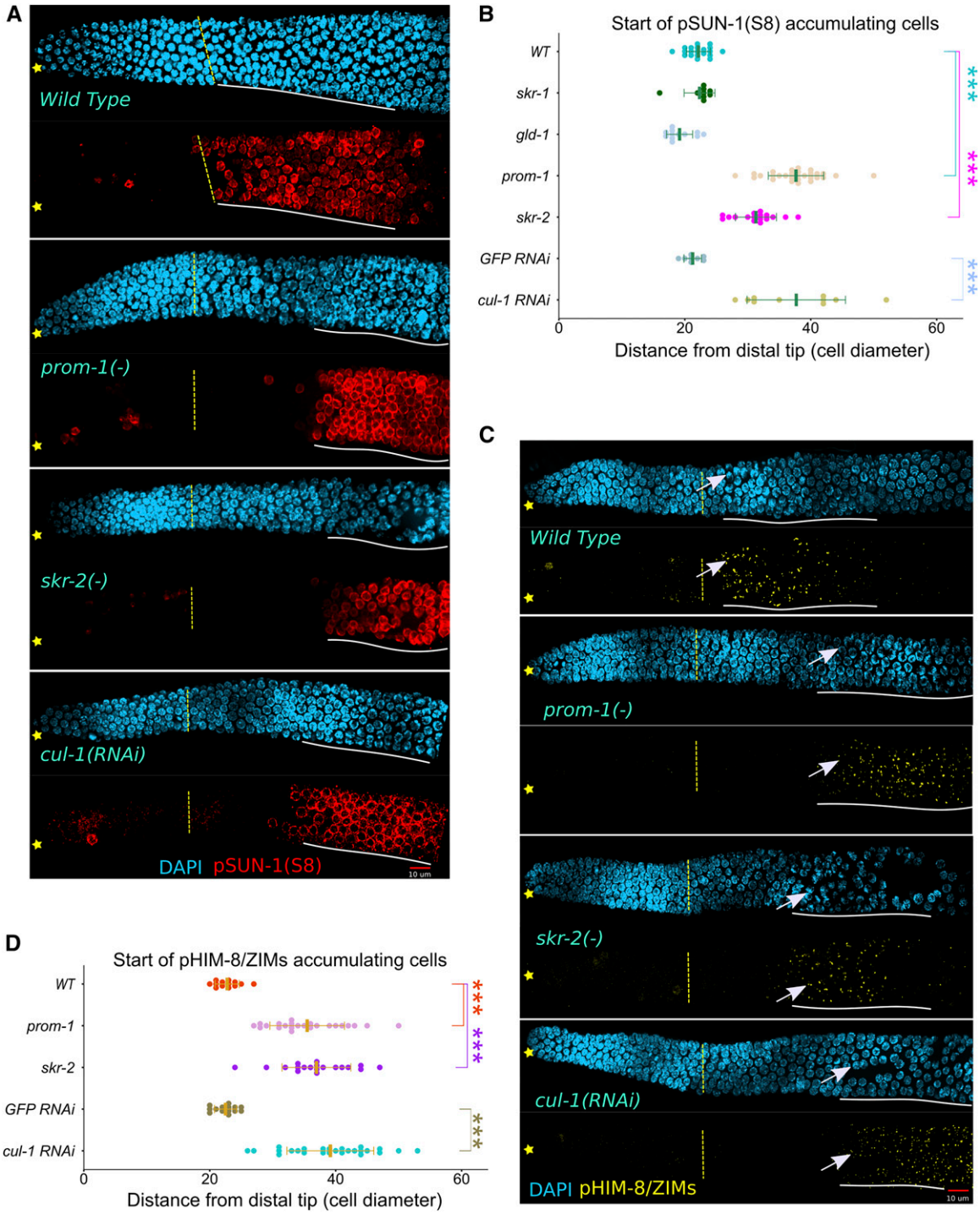

Figure 3 CHK-2 activity is absent at meiotic entry in SCF^{PROM-1} mutant germlines. (A and C) Images of (A) pSUN-1(Ser8)-stained (red) and (C) pHIM-8/ZIMs-stained (yellow) distal germlines from dissected young-adult hermaphrodites, costained with DAPI (cyan) for the indicated genotype. ☆ indicates distal gonadal end. Dashed yellow lines indicate position of overt meiotic entry. Solid white lines indicate start and positions of (A) pSUN-1(Ser8) and (C) pHIM-8/ZIMs accumulation. →'s indicate nuclei with pHIM-8/ZIMs staining. Note, pSUN-8 also appears on M-phase cells in the progenitor zone. (B and D) Graph showing distance, in cell diameters, from DT of the germline to first cell row of (B) pSUN-1(Ser8)-positive nuclei and (D) pHIM-8/ZIMs-positive nuclei (beginning of white lines in A and C above) for young-adult hermaphrodites of the indicated genotype. Data are plotted as horizontal dot plots with each dot representing length in cell diameters to the beginning of staining for one gonad. Thick vertical lines represent mean and horizontal lines represent mean ± SD. *P*-value ≤ 0.01 (*); ≤ 0.001 (**); ≤ 0.0001 (***); > 0.01 non-significant (NS.). WT, wild type.

proteins that have mitotic cell cycle functions. To test this, we selected pCDC-6, an essential replication factor that has been reported to be phosphorylated by CYE-1/Cdk2 (Mailand and Diffley 2005); WAPL-1, which functions in removal of cohesin from chromatin in mitotically cycling cells (Gandhi *et al.* 2006; Kueng *et al.* 2006); and KNL-2, a kinetochore assembly protein (Maddox *et al.* 2007).

pCDC-6 is present in the nucleolus of all progenitor zone nuclei in wild-type germlines and is downregulated at leptotene–zygotene (Kim and Kipreos 2007; Fox *et al.* 2011). In *prom-1* and *skr-2* young-adult hermaphrodite mutant germlines, pCDC-6 failed to be downregulated at meiotic entry and extends to ~40 cell diameters from the DT, compared to ~24 cell diameters in wild type (Figure 4, A and C). WAPL-1 and KNL-2 also accumulate in all progenitor zone nuclei and are downregulated at meiotic entry (Crawley *et al.* 2016; A. Desai, personal communication; Figure 4B, Figure S6). We found that both WAPL-1 and KNL-2 failed to be downregulated in the extended early leptotene region of SCF^{PROM-1} mutant germlines (Figure 4, B, D, and E, and Figure S6). Thus, all mitotic cell cycle proteins tested failed to be downregulated at meiotic entry in SCF^{PROM-1} mutant germlines but eventually are downregulated ~40 cell diameters from the DT. Therefore, SCF^{PROM-1} loss-of-function germlines show a distinctive phenotype: cells proximal to the progenitor zone enter meiosis (Figure S3) but fail to downregulate at least four, normally progenitor zone-restricted mitotic cell cycle proteins.

REC-8 has been widely used as a progenitor zone marker and thus its behavior in SCF^{PROM-1} loss of function is of interest. REC-8 is nucleoplasmic in progenitor zone cells and loads onto the chromosome axes as thin threads at meiotic entry (Pasierbek *et al.* 2001); under our mild fixation conditions, only the nucleoplasmic progenitor zone staining is observed (Hansen *et al.* 2004b). Similar to CYE-1 and other mitotic proteins listed above, the nucleoplasmic REC-8 shows an extended accumulation in *prom-1* and *skr-2* mutant germlines (Figure 4F).

While cells in the extended early leptotene region of SCF^{PROM-1} mutant germlines accumulate a number of mitotic cell cycle proteins (*e.g.*, CYE-1), they are not mitotically cycling (Figure S3, D and E). One possibility as to why they are not cycling could be that although CYE-1 is present, CYE-1–CDK-2 is not active. To examine this, we looked at the CIP/KIP family of cyclin-dependent kinase inhibitors (CKIs), which are known negative regulators of CYE-1–Cdk2 (Sherr and Roberts 1999). The *C. elegans* genome encodes two CKIs: *cki-1* and *cki-2* (Hong *et al.* 1998). Of these, only CKI-2 accumulates in the distal germline (Kalchhauser *et al.* 2011), although *cki-2* mutant germ cells enter meiosis normally. If CKI-2 functions to inhibit ectopic CYE-1–CDK-2 activity in SCF^{PROM-1} loss-of-function germlines, then loss of *cki-2* in SCF^{PROM-1} may lead to mitotic cycling in cells with ectopic CYE-1. Following 4 hr of labeling, the EdU zone in *prom-1*; *cki-2* germlines remain similar to wild type (Figure S7). Since loss of *cki-2* restores the progenitor zone in *fbf-1 fbf-2* double mutant gonads only at 25° (Kalchhauser *et al.* 2011), we also examined *prom-1*; *cki-2* double mutant germlines at 25° and found no extension of the EdU zone in the double mutant germlines (Figure S7). We conclude that the absence of mitotic cycling in the extended early leptotene region of SCF^{PROM-1} is not due to inhibition of CYE-1–CDK-2 by CKI-2.

Male SCF^{PROM-1} mutants have an extended zone of mitotically cycling cells

We next asked if the homologous chromosome pairing defect and ectopic accumulation of mitotic cell cycle proteins in SCF^{PROM-1} mutant germlines is hermaphrodite specific or also occurs in males. We used antibodies against pHIM-8/ZIMs as a readout to assess CHK-2 activity. Similar to SCF^{PROM-1} mutant hermaphrodites, the appearance of pHIM-8/ZIMs was delayed by >10 cell diameters in mutant male germlines, compared to control, indicating that SCF^{PROM-1} mutants lacked CHK-2 activity at the meiotic entry (Figure 5A). We also found that male germlines of SCF^{PROM-1} mutants failed to downregulate mitotic cell cycle proteins CYE-1, pCDC-6, and WAPL-1, as well as nucleoplasmic REC-8, at meiotic entry, similar to what we observed in hermaphrodites (Figure S8, A–D, unpublished results).

Unexpectedly, we found that both *prom-1* and *skr-2* males have an extended zone of mitotically cycling cells. This was indicated by (1) *prom-1* and *skr-2* mutant male germlines having continuous zones of EdU-labeled cells that were significantly longer than in wild-type male germlines (Figure 5, B and C); and (2) the extended EdU zone, called region 2, having ectopic M-phase nuclei (identified as pH3 positive) that were essentially all colabeled with EdU (Figure 5, B and D), indicating that these cells were mitotically cycling (Figure S9). To test if the extended EdU zone in *prom-1* males was due to the germline having the male fate, we employed the *fog-1* null sex determination mutant to feminize the germline but not the soma of males (Barton and Kimble 1990) and examined the *fog-1 prom-1* double mutant. Although CYE-1 remained ectopic (Figure S8A), the continuous EdU zone was reduced to nearly wild-type level (Figure 5C). Thus, the adult male germline requires SCF^{PROM-1} to inhibit mitotic cell cycling at meiotic entry, unlike female germ cells in the adult hermaphrodite or the feminized germline of somatic males.

SCF^{PROM-1} functions redundantly with the GLD-1 pathway to promote meiotic entry and inhibit mitotic cycling

SCF^{PROM-1} has properties suggesting it functions in the control of meiotic entry: it is required for timely homologous chromosome pairing and downregulation of mitotic cell cycle protein levels in hermaphrodites and males, and it is necessary for the inhibition of mitotic cycling at meiotic entry in males. Previous work indicated that there are additional activities that function in parallel to GLD-1 and GLD-2 pathways to promote meiotic entry; in *gld-2 gld-1* double mutants the germline is tumorous, but some cells enter

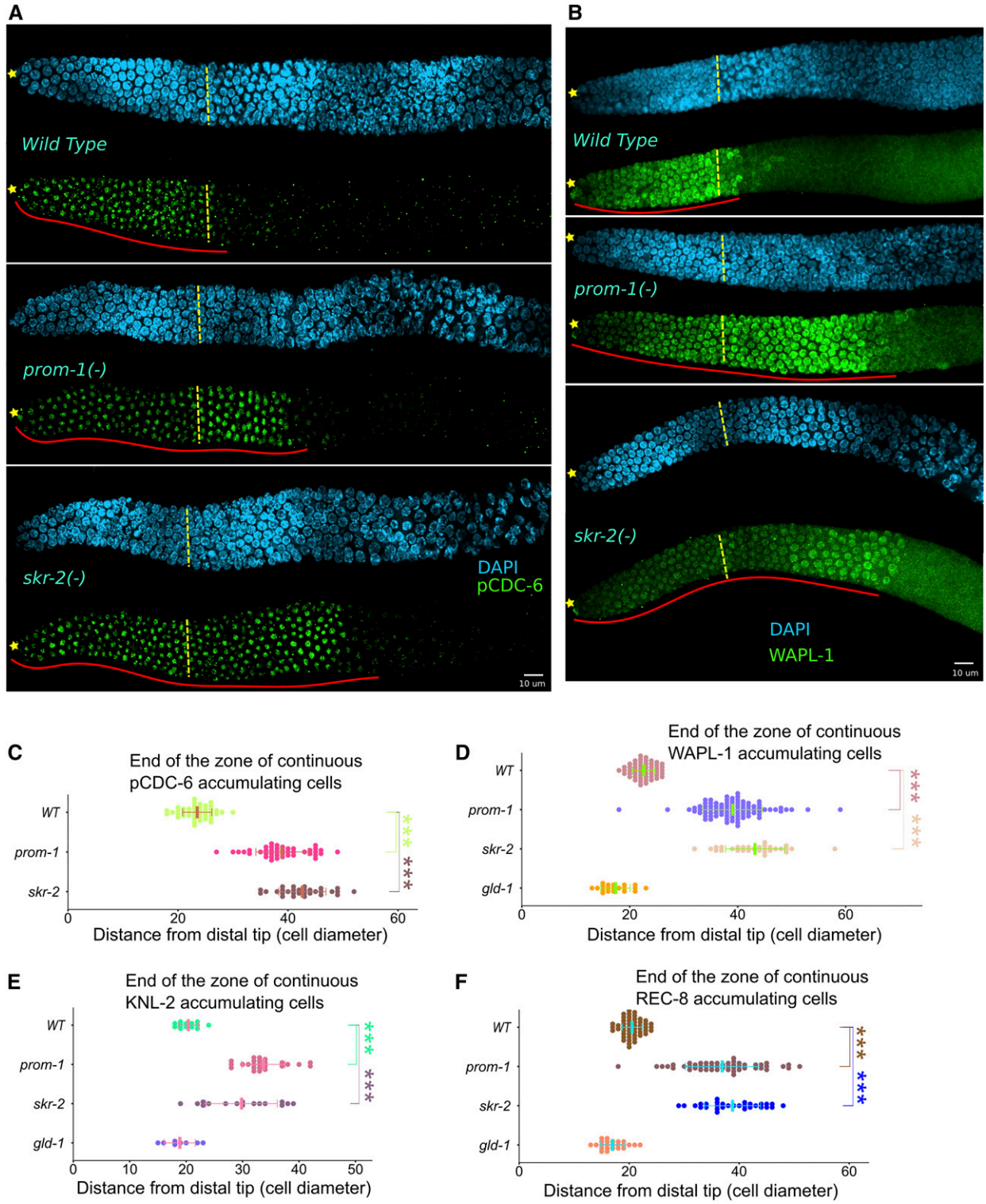

Figure 4 Failure to downregulate mitotic cell cycle proteins in SCF^{PROM-1} mutant germlines. (A and B) Images of (A) pCDC-6 (green) and (B) WAPL-1 (green) stained distal germlines from dissected young-adult hermaphrodites, costained with DAPI (cyan) for the indicated genotype. ☆ indicates distal gonadal end. Dashed yellow lines indicate position of overt meiotic entry. Solid red lines indicate zone of continuous (A) pCDC-6 and (B) WAPL-1 protein accumulation. (C–F) Graph showing distance, in cell diameters, from DT of the germline to last cell row where the majority of nuclei are positive for (C) pCDC-6, (D) WAPL-1, (E) KNL-2, and (F) nucleoplasmic REC-8 for the indicated genotype. Data are plotted as horizontal dot plots with each dot representing length in cell diameter for one gonad. Thick vertical lines represent mean and horizontal lines represent mean ± SD. *P*-value ≤ 0.01 (*); ≤ 0.001 (**); ≤ 0.0001 (***); > 0.01 non-significant (NS.). WT, wild type.

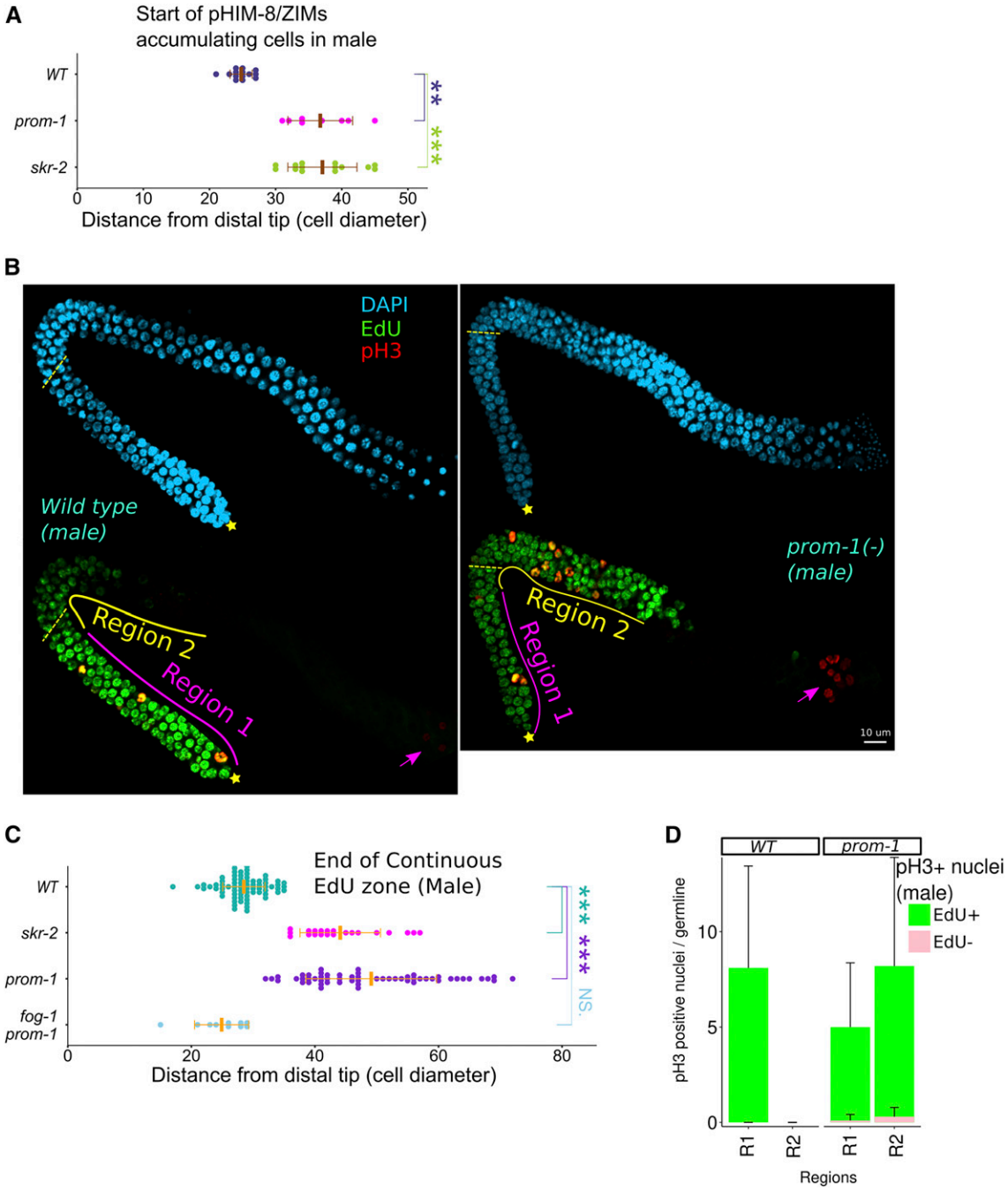

Figure 5 Extended zone of mitotically cycling cells in SCF^{PROM-1} mutant male germlines. (A and C) Graph showing distance, in cell diameters, from the DT of the (B) continuous EdU zone and the (D) first appearance of pHIM-8/ZIMs foci in male germlines of the indicated genotype. Data are plotted as horizontal dot plots with each dot representing length in cell diameters to (A) the beginning of the zone of pHIM-8/Zim or (C) the end of the continuous EdU zone for one germline. Thick vertical lines represent mean and horizontal lines represent mean ± SD. *P*-value ≤ 0.01 (*); ≤ 0.001 (**); ≤ 0.0001 (***); > 0.01 non-significant (NS.). (B) Images of 4-hr EdU-labeled (green), pH3-stained (red) distal germlines from dissected young-adult males costained with DAPI (cyan) for the indicated genotype. ☆ indicates distal gonadal end. Dashed yellow lines indicate position of overt meiotic entry. Solid lines: region 1 (magenta line) is first 20 cell diameter from distal end of the gonad, region 2 is defined as starting from the proximal end of region 1 to ~40 cell diameter or the end of continuous EdU zone (yellow line). → indicates pH3-stained spermatocytes undergoing meiosis I or II divisions. (D) Bar graph showing number of pH3-positive nuclei that are EdU+ or EdU− in regions 1 and 2 (see B above) in male germlines of the indicated genotype. EdU+ pH3-positive cells are considered to be mitotically cycling (see Figure S9). Data are shown for 10 germlines for each genotype. Error bars, SD. WT, wild type.

meiosis (Hansen *et al.* 2004b). Importantly, CYE-1 is down-regulated in the few cells that enter meiosis in *gld-2 gld-1* mutants (Fox *et al.* 2011). Similarly, we found that WAPL-1 and pCDC-6 are also downregulated in the few clusters of meiotic cells in *gld-2 gld-1* tumorous germlines (Figure S10). These results indicate that CYE-1, WAPL-1, and pCDC-6 are

downregulated at meiotic entry by a mechanism that is independent of the GLD-1 and GLD-2 pathways.

This leads to the hypothesis that SCF^{PROM-1} acts in parallel to the GLD-1 and GLD-2 pathways to promote meiotic entry. If so, then loss of SCF^{PROM-1} should (1) show a synthetic overproliferation phenotype with GLD-1 and with GLD-2 pathway gene mutations, (2) function downstream of GLP-1/Notch signaling, and (3) enhance the meiotic entry defect of GLD-1 and GLD-2 pathway double mutants.

We first examined the interaction between SCF^{PROM-1} and the GLD-1 pathway genes *gld-1* and *nos-3*. Meiotic entry is normal in *gld-1* single null mutant germlines (Figure 2B, Figure 3B, Figure 4, D–F, and Figure S3), but they display proximal overproliferation due to female/oogenic, but not male/spermatogenic, pachytene cells dedifferentiating and returning to mitotic cell cycling (Francis *et al.* 1995a,b; Biedermann *et al.* 2009). The experiments below were designed to determine if SCF^{PROM-1} mutants caused a synthetic ectopic proliferation phenotype in an already tumorous *gld-1* mutant young-adult hermaphrodite, and to determine if the ectopic proliferation arose from continued mitotic cycling or a return to mitosis from meiotic prophase cells.

We used 4-hr EdU labeling in young adults to identify cells that were in S phase during at least part of the labeling period (*Materials and Methods*; Figure S9). In contrast to *gld-1* or *prom-1* single mutant gonads, *gld-1 prom-1* double mutants exhibited an extended region of S-phase germ cells, as shown by the length of the continuous EdU zone (Figure 6, A and B). Similarly, an extended EdU zone was observed for *gld-1 skr-2* double mutants (Figure 6B). Although we never observed an EdU zone in *gld-1* germlines extending beyond 30 cell diameters ($n = 65$), 3/20 gonads in *gld-1*; *cul-1*(*RNAi*) worms had a continuous EdU zone length of >40 (Figure S11A). We also observed a modest, but statistically significant, extension of EdU zone in *prom-1*; *nos-3* double mutant germlines (Figure 6B; unpublished observation).

To determine if the extended EdU zone in *gld-1 prom-1* double mutants is due to cells undergoing mitotic S phase, rather than meiotic S phase, we colabeled germlines with EdU and anti-pH3 antibody to mark M-phase nuclei. For quantitative analysis, germlines were divided into regions 1 through 5 (Figure S11B). The pH3-positive nuclei were regionally counted and, based on EdU colocalization, were assigned as either EdU+, which we infer are mitotically cycling cells, or are EdU−, which may be cells that have returned to the mitotic cell cycle (Figure S9). Region 1 corresponds to the progenitor zone; in both *gld-1* and *gld-1 prom-1* mutant germlines, pH3 nuclei were almost exclusively EdU+, consistent with cells cycling mitotically (Figure S11, B and C). Region 2 in *gld-1* single mutants comprised leptotene, zygotene, and early pachytene cells and displayed very few pH3-positive nuclei, the majority of which were present at the proximal end and were not colabeled with EdU, suggesting that these few M-phase cells arose from pachytene cells that returned to mitosis. Region 2 in *gld-1 prom-1* mutants mainly comprised the extended continuous EdU zone and contained, on average, 10 pH3-positive nuclei that were colabeled with EdU, which we interpret as mitotically cycling cells. Therefore, we conclude that *gld-1 prom-1* young-adult double mutants display a synthetic overproliferation phenotype. Regions 3 and 4 in *gld-1* and *gld-1 prom-1* mutants contained mostly pH3 nuclei that are EdU−, which we interpret as cells that returned to mitosis, consistent with previous characterization of *gld-1* null mutants (Francis *et al.* 1995a,b). Finally, region 5 of *gld-1* and *gld-1 prom-1* mutants contained pH3 nuclei: a minority were EdU−, and thus likely arose due to a return to mitosis, and a majority were EdU+ and were likely to be mitotically cycling cells that arose from an earlier return to mitosis events (Francis *et al.* 1995a,b). To understand the genesis of the overproliferation phenotype in region 5, we examined L4 animals and found that while *gld-1* single mutants had EdU-labeled nuclei largely restricted to the distal part of the germline, *gld-1 prom-1* double mutants had EdU-labeled nuclei throughout. Furthermore, in the proximal region of *gld-1* germlines, 50% of pH3 nuclei were EdU− (from 20 nuclei, 21 gonads), consistent with a return to mitosis (Francis *et al.* 1995b); while in *gld-1 prom-1* >99% of pH3 nuclei were EdU+ (from 161 nuclei, 22 gonads), suggesting a failure of proximal germ cells to enter meiosis and instead were due to continuous mitotic cell cycling (unpublished result).

The synthetic overproliferation phenotype revealed by the extended distal EdU zone in *gld-1 prom-1* double mutant young adults could either be due to cells that have continued mitotic cycling from the progenitor zone, or cells that returned to mitosis at an earlier stage of development and were then mitotically cycling, analogous to region 5 in *gld-1* single mutants. To distinguish between these two possibilities, we blocked meiotic prophase progression using a null mutation in *mek-2*, which arrests germ cells in pachytene and prevents a return to mitosis in *gld-1* mutant hermaphrodite germlines (Lee and Schedl 2010). M-phase cells were absent in *mek-2 gld-1* double mutants in region 2 as well as in region 3 (Figure S11D), consistent with blocking a return to mitosis. In contrast, *mek-2 gld-1 prom-1* triple mutants had numerous M-phase nuclei that were EdU+ in region 2, indicating that these cells did not arise from germ cells entering meiosis, progressing to pachytene, and then returning to mitosis because such germ cells would have been arrested in pachytene. The EdU zone lengths in *mek-2 gld-1 prom-1* germlines were still extended compared to *mek-2 gld-1* germlines, indicating that the extended EdU zone is due to continued mitotic cycling (Figure S11E). The EdU zones of both *mek-2 gld-1* and *mek-2 gld-1 prom-1* mutants, however, were smaller than *gld-1* and *gld-1 prom-1* mutant germlines, respectively. Also, overall pH3 nuclei counts were fewer in *mek-2* double and triple mutants compared to non-*mek-2* counterparts (Figure S11, D and E). This reduction in EdU zone length, as well as total M-phase nuclei, is likely due to the previously described role of *mek-2* in promoting robust mitotic cell cycling and progenitor zone length (Lee *et al.* 2007).

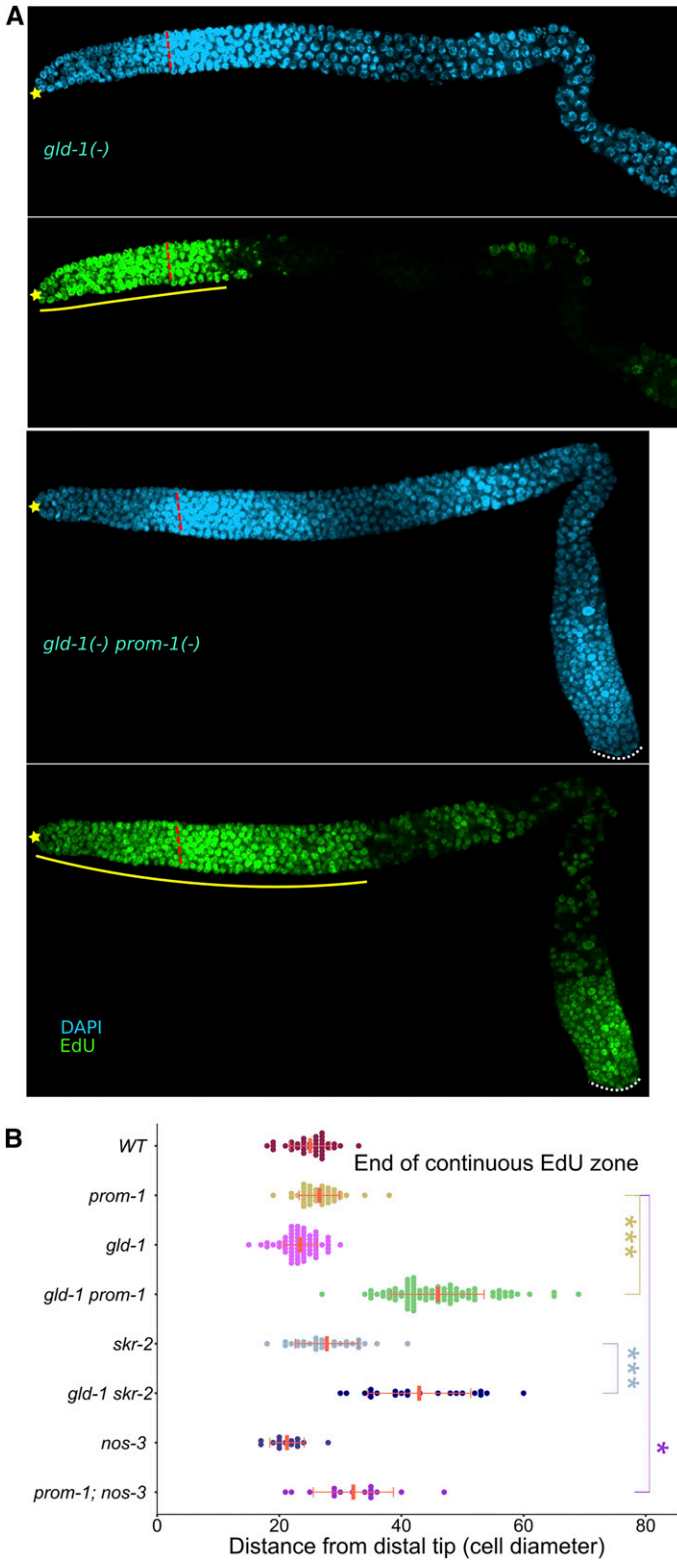

Figure 6 SCF^{PROM-1} functions redundantly with GLD-1 to inhibit ectopic mitotic activity. (A) Images of 4-hr EdU labeled (green), costained for DNA (DAPI, cyan), germlines from dissected young-adult hermaphrodites of the indicated genotype. ☆ indicates distal gonadal end. Dashed red lines indicate position of overt meiotic entry. Solid yellow lines indicate zone of continuous EdU-labeled cells. Dotted white lines indicate proximal end of the germline. (B) Graph showing continuous EdU zone length, in cell diameters from the DT to the proximal end, for the indicated genotype of young-adult hermaphrodite germlines. Data are plotted as horizontal dot plots with each dot representing length in cell diameter for one gonad. Thick vertical lines represent mean and horizontal lines represent mean ± SD. *P*-value ≤ 0.01 (*); ≤ 0.001 (**); ≤ 0.0001 (***); > 0.01 non-significant (NS.). WT, wild type.

Together, these results strongly suggest that the extended zone of mitotically dividing cells in *gld-1 prom-1* mutants is due to progenitor zone cells that have continued to cycle mitotically in the region where germ cells should have entered meiosis.

Overproliferation phenotypes that arise from a failure of germ cells to enter meiosis are independent of germline sexual fate (Berry *et al.* 1997; Kadyk and Kimble 1998; Hansen *et al.* 2004b), while overproliferation that arises from a return to mitosis occurs in only one sex, the oogenic germline with *gld-1*,

Table 1 *gld-1 prom-1* double mutant overproliferation phenotype is not germline sex specific (at 25°)

Genotype	Sex	Only sperm (%)	Overproliferation (%)[a]	*n*[b]
gld-1; *fem-3*(*gf*)	Hermaphrodite	74	26[c]	69
	Male	9	91[c]	22
gld-1 prom-1/+; *fem-3*(*gf*)	Hermaphrodite	100	0	35
gld-1 prom-1; *fem-3*(*gf*)	Hermaphrodite	0	100	77
	Male	0	100	11
gld-1 prom-1	Hermaphrodite	0	100	32
	Male	0	100	7

[a] Animals 18 hr past mid-L4 were dissected and ascertained for overproliferation through REC-8 and HIM-3 staining as well as chromatin morphology.
[b] Number of gonad arms analyzed.
[c] A proximal tumor after a zone of sperm, a phenotype associated with *gld-1* mutant males grown at 25° (Priti and Subramaniam 2015).

and the spematogenic germline with *puf-8* (Francis *et al.* 1995a; Subramaniam and Seydoux 2003). If SCF^{PROM-1} functions to promote meiotic entry, then we expect that the synthetic overproliferation phenotype observed in the *gld-1 prom-1* double mutant should be independent of germline sexual fate. We first asked if masculinization of the germline in *gld-1 prom-1* hermaphrodites with the temperature-sensitive *fem-3*(*gf*) allele at restrictive temperature (25°) (Barton *et al.* 1987) alters the synthetic overproliferation phenotype. Whereas most germlines of *gld-1*; *fem-3*(*gf*) showed a masculinization of the germline phenotype at the restrictive temperature, suppressing the proximal overproliferation (Table 1; also see Priti and Subramaniam 2015), 100% of the *gld-1 prom-1*; *fem-3*(*gf*) triple mutant hermaphrodites remained tumorous (Table 1). To further investigate if *gld-1 prom-1* overproliferation is germline sex specific, we next examined the overproliferation phenotype in *gld-1 prom-1* young-adult males. EdU+ nuclei were present throughout most of the germline (Figure S12A, Table 2), rather than being limited to the progenitor zone in *gld-1* single mutants or the extended distal zone of mitotically cycling cells in *prom-1* single mutants (Figure 5, B–D). A similar but weaker overproliferation phenotype was seen in *gld-1 skr-2* male germlines (Table 2, unpublished results). Masculinizing the germline of *gld-1 prom-1* males with *fem-3*(*gf*) did not suppress the tumor, precluding the possibility that the tumor in males is due to a feminized germline (Table 1; Francis *et al.* 1995b). Thus, the synthetic overproliferation found in SCF^{PROM-1} *gld-1* double mutants occurs independently of the germ cell sexual fate, as is observed in GLD-1 GLD-2 pathway double mutants.

CYE-1 is expressed in the progenitor zone, downregulated from leptotene to late pachytene, and then accumulates to high levels in growing oocytes (Biedermann *et al.* 2009; Fox *et al.* 2011). In contrast, CYE-1 is found throughout the germline in *gld-1 prom-1* double mutants (Fox *et al.* 2011), suggesting that SCF^{PROM-1} and GLD-1 are together sufficient for inhibiting CYE-1 accumulation from leptotene to late pachytene. In support of this conclusion, we found CYE-1 throughout the germline in *gld-1 skr-2* and *gld-1*; *cul-1* RNAi hermaphrodites as well as *gld-1 prom-1* males (Figure S11A and Figure S12A; unpublished results). KNL-2 and WAPL-1 have a similar pattern of accumulation in wild-type hermaphrodites as CYE-1. We found that while KNL-2 and WAPL-1 levels were downregulated at meiotic entry in *gld-1* single mutants (Figure 2B and Figure 4, D and E), they were found throughout the germline of *gld-1 prom-1* double mutants (Figure S12, B and C). Thus, SCF^{PROM-1} and GLD-1 function together in downregulation of multiple mitotic cell cycle proteins from leptotene to late pachytene.

SCF^{PROM-1} *gld-1* double mutants display an extended zone of mitotically cycling germ cells containing ectopic mitotic cell cycle proteins; do germ cells nevertheless attempt to enter meiosis? We found that spatial accumulation of meiotic chromosome axis proteins HIM-3 and meiotic cohesins COH-3/4 was similar to wild type, appearing at ~20 cell diameters from the distal end in *gld-1 prom-1* mutants (Figure S13, A and B). However, while loading of COH-3/4 onto chromosomes was largely normal (although with reduced staining intensity: Figure S13B), HIM-3 was localized primarily to the cytoplasm/nucleoplasm in the region of extended mitotically cycling cells, with increased chromatin association more proximally (Figure S13A). In wild type, GLD-1 accumulates at low levels in the region where germline stem cells reside and then rises in a sigmoidal pattern ~20-fold, peaking as germ cells enter meiosis (Brenner and Schedl 2016). To determine if GLD-1 accumulates in the extended zone of mitotically cycling cells in *gld-1 prom-1* mutant germlines, we employed the *gld-1*(*q361*) allele, which produces stable but not functional GLD-1 (Jones and Schedl 1995; Hansen *et al.* 2004a). We found that in *gld-1*(*q361*) *prom-1* double mutants, GLD-1 shows a similar rise as observed in wild type (Figure S14). Thus, while *gld-1 prom-1* double mutant germlines have turned "on" part of the meiotic entry program at the appropriate location in the germline—at least with respect to HIM-3, COH-3/4, and GLD-1—they have failed to turn "off" the mitotic program, resulting in an extended zone of mitotically cycling cells. Although we have not examined all possible double mutants with GLD-1 pathway and SCF^{PROM-1} components, it is likely that our findings using primarily *gld-1 prom-1* can be extended to the remaining genes. We conclude that SCF^{PROM-1} functions redundantly with the GLD-1 pathway to inhibit mitotic cell cycling at meiotic entry.

SCF^{PROM-1} acts redundantly with the GLD-2 pathway to promote meiotic entry and inhibit mitotic cycling

The synthetic interaction of SCF^{PROM-1} components with GLD-1 pathway genes suggests that SCF^{PROM-1} could function in

Table 2 *gld-1*(−) SCF^{PROM-1}(−) male and hermaphrodite phenotype at 20°

Genotype	Sex	Only sperm (%)	Overproliferation (%)[a]	n^b
gld-1	Hermaphrodite	0	100	>100
	Male	100	0	>100
gld-1 prom-1	Hermaphrodite	0	100	>100
	Male	0	100	>100
gld-1 skr-2	Hermaphrodite	0	100	>100
	Male	0	100	10

[a] Young adult worms were assessed for overproliferation phenotype by EdU incorporation and pH3 staining (see Figure 5B).
[b] Number of gonad arms analyzed.

the GLD-2 pathway or in a third pathway parallel to the GLD-1 and GLD-2 pathways. If in the GLD-2 pathway, we would expect that SCF^{PROM-1} GLD-2 pathway double mutants would not exhibit synthetic overproliferation; if in a third pathway, overproliferation in double mutants would be expected. We tested SCF^{PROM-1} interaction with the GLD-2 pathway by making double mutants of *prom-1* or *skr-2* with *gld-2* or *gld-3*. *gld-2* mutant worms are defective in gametogenesis and exhibit a very low percentage proximal overproliferation (Kadyk and Kimble 1998). *gld-3* mutant germlines are feminized and have incompletely penetrant abnormalities in oogenesis (Eckmann *et al.* 2002; Green *et al.* 2011). Meiotic entry is essentially normal in both the *gld-2* and *gld-3* single null mutant germlines. However, animals lacking either *gld-2* or *gld-3* and one GLD-1 pathway gene are defective in meiotic entry and form synthetic germline tumors (Kadyk and Kimble 1998; Eckmann *et al.* 2002; Hansen *et al.* 2004a).

For both *gld-2 prom-1* and *prom-1*; *gld-3* germlines, EdU labeling revealed overproliferation, with ectopic S phase cells mostly residing in the proximal arm of young-adult germlines (Figure 7, Figure S15A, and Table 3). A less-penetrant overproliferation phenotype was observed in *gld-2 skr-2* and *skr-2*; *gld-3* double mutant germlines (Table 3). Unlike *gld-1* SCF^{PROM-1} double mutants, *gld-2* or *gld-3* double mutants with *prom-1 or skr-2* do not show a continuous extended zone of EdU-labeled cells in young adults (Figure S15B). However, a significant number of scattered EdU+ cells were qualitatively observed proximal to the progenitor zone, especially in *gld-2 prom-1* and *gld-2 skr-2* as compared to *gld-2*, *gld-3*, *prom-1*, and *skr-2* single mutant germlines (Figure 7; unpublished results). In addition, we examined interaction with GLD-4, a subcomponent of the GLD-2 pathway (Millonigg *et al.* 2014), where we found that *gld-4* null displayed increased sterility penetrance at 25° (unpublished observation). *gld-4 prom-1* double mutant hermaphrodite germlines showed an overproliferation phenotype at 25° (Table 3), but not at 20°.

Costaining for pH3 and EdU of *gld-2 prom-1* or *gld-2 skr-2* double mutant young-adult germlines revealed that M-phase nuclei were EdU+ in the proximal germline, indicating active mitotic cycling (Figure S15C and unpublished results). To assess the genesis of overproliferation in the proximal germline, we colabeled *gld-2* and *gld-2 prom-1* germlines, at the L4 stage, a few hours after the first proximal germ cells enter meiosis in mid-L3 in wild type. In *gld-2* single mutant germlines, pH3-positive and EdU+ nuclei were confined to the distal progenitor zone; but in *gld-2 prom-1*, EdU+ nuclei were present throughout the germline (Figure S16A). In *gld-2 prom-1* L4 germlines, >99% of M-phase nuclei were colabeled with EdU (458 nuclei, 24 gonads), indicating that a significant number of germ cells were mitotically cycling and failed to enter meiosis. As worms grew older, the mitotically cycling cells in the double mutant germlines eventually separated into distal (progenitor zone) and proximal tumor EdU(+) regions with meiotic prophase cells in between. This likely explains the presence of scattered S-phase cells in the region proximal to the progenitor zone in young-adult double mutants (Figure 7). Together, these results suggest that SCF^{PROM-1} acts in parallel with the GLD-2 pathway to promote meiotic entry and/or inhibit proliferation.

In the *gld-2 prom-1* double mutant, unlike the *gld-1 prom-1* double mutant, accumulation of HIM-3 and COH-3/4 was mutually exclusive from EdU+ mitotically cycling cells, based on a 30-min EdU pulse labeling (Figure S16, B and C), and the typical HIM-3 chromosome axis staining was observed. Similarly, accumulation and chromosome axis staining for HIM-3 was mutually exclusive from EdU+ mitotic cycling cells in *prom-1*; *gld-3* double mutant germlines (unpublished results). Therefore, there are differences in the extent to which aspects of the meiotic program are initiated in ectopic mitotic cycling cells in *gld-1 prom-1 vs. gld-2 prom-1* double mutants.

CYE-1 is downregulated in *gld-2* and *gld-3* single mutant germlines upon meiotic entry and only accumulates again in nuclei corresponding to late pachytene, similar to the pattern in wild-type germlines (Figure 7, Figure S15A, and Figure S16D). In *gld-3 prom-1* (as well as *gld-2 skr-2* and *gld-3 skr-2*), CYE-1 accumulation was extended into meiotic prophase, similar to the accumulation pattern in SCF^{PROM-1} single mutants (Figure 7, Figure S15A, and Figure S16D). In contrast, CYE-1 levels were high throughout the germline of *gld-2 prom-1* mutant germlines (Figure 7). This indicates that GLD-2 functions redundantly with PROM-1 to inhibit CYE-1 accumulation, and that GLD-2 and GLD-3 are not completely functionally equivalent, consistent with previous reports (Mantina *et al.* 2009; Kerins *et al.* 2010; Millonigg *et al.* 2014). Also, since CYE-1 is not expressed throughout the germline of *gld-2 skr-2* double mutants, *skr-2* loss does not completely mimic *prom-1* loss (also see below). Since SCF^{PROM-1} GLD-2 pathway double mutants have a synthetic overproliferation, SCF^{PROM-1} does not function in the GLD-2

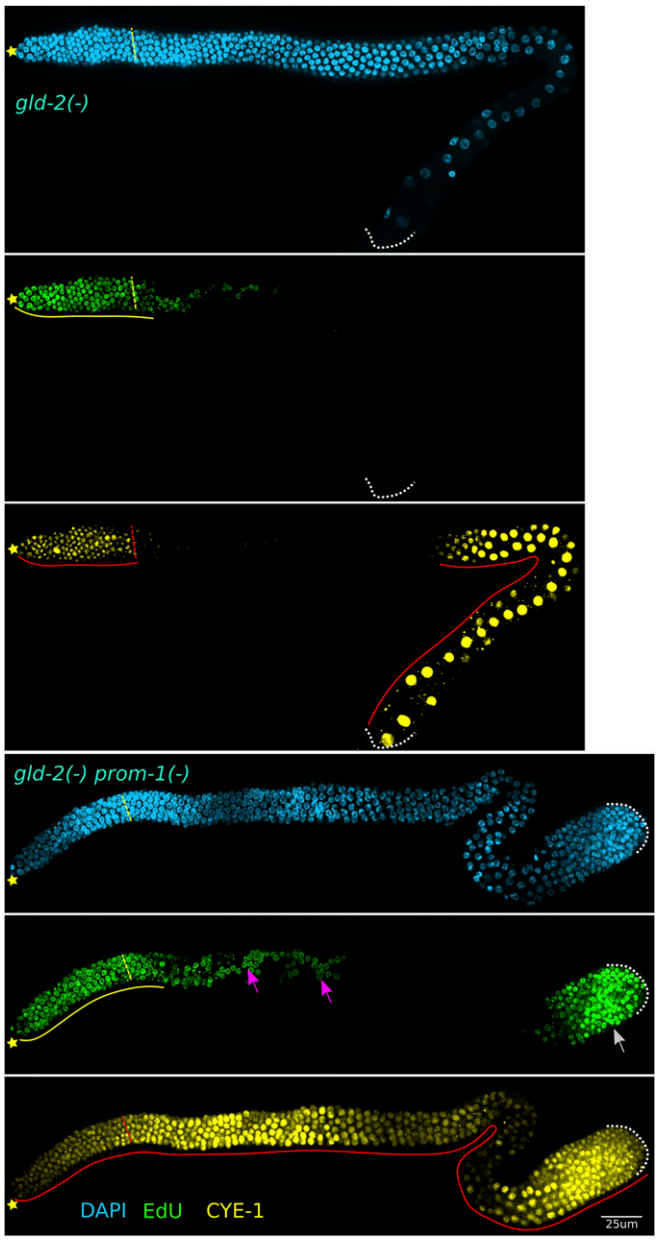

Figure 7 SCF^{PROM-1} loss of function in combination with *gld-2* null results in synthetic overproliferation. Images of dissected germlines from young-adult *gld-2* (top) and *gld-2 prom-1* (bottom) mutant hermaphrodites, labeled with EdU for 4 hr (green), and costained for CYE-1 (yellow) and DAPI (cyan). ☆ indicates distal gonadal end. Dashed yellow (top) or red (bottom) lines indicate position of overt meiotic entry. Solid yellow lines indicate continuous EdU zone. Solid red lines indicate continuous CYE-1 accumulation. White arrow indicates proximal proliferation; pink arrow indicates stray EdU+ cells proximal to progenitor zone. Dotted white lines indicates proximal end of the germlines.

pathway, but rather likely functions in a third pathway redundant with the GLD-1 and GLD-2 pathways.

SCF^{PROM-1} acts downstream of GLP-1 Notch signaling to inhibit germ cell proliferation

The GLD-1 and GLD-2 pathways both function downstream of GLP-1 Notch signaling (Kadyk and Kimble 1998; Eckmann *et al.* 2004; Hansen *et al.* 2004a); therefore, if SCF^{PROM-1} functions in parallel with the GLD-1 and GLD-2 pathways, it should also function downstream of GLP-1 Notch signaling. To test this, we asked if the overproliferation phenotypes in double mutants between *gld-1*, *gld-2*, or *gld-3* and SCF^{PROM-1} are epistatic to the premature meiotic entry phenotype of the *glp-1* null mutant. Complete loss of GLP-1 function results in all germ cells prematurely entering meiosis, forming a few sperm (Austin and Kimble 1987). Double mutants between *glp-1* null and a single mutant from either the GLD-1 or GLD-2 pathway show a similar premature meiotic entry phenotype (Francis *et al.* 1995b; Kadyk and Kimble 1998; Hansen *et al.* 2004a). We constructed triple mutants with *glp-1* and one of *gld-1*/*gld-2*/*gld-3* and either *prom-1* or *skr-2*, and found that young-adult germlines contained significantly more cells than their *gld*; *glp-1* double mutant counterparts (Table 3). We further examined their germlines by costaining for EdU (4-hr labeling) and pH3 and found that all triple mutant germlines had mitotically cycling cells, with the exception of *gld-2 skr-2*; *glp-1* (Figure 8, A and B, and Table 3). In all cases, triple mutant germlines contained some HIM-3-positive cells interspersed with EdU+ cells (unpublished results). To determine if the tumors in *gld-1 prom-1*; *glp-1* and *gld-2 prom-1*; *glp-1* germlines could arise from cells failing to enter meiosis, rather than entering into meiosis and then returning to mitosis earlier in development, we analyzed mitotic and meiotic cells during larval development. In wild-type hermaphrodites, germ cells begin to enter meiosis at mid-L3 (Kimble and White 1981; Hansen *et al.* 2004b). In contrast, in *glp-1* single and *gld-1*; *glp-1* and *gld-2*; *glp-1* double mutants, all germ cells prematurely enter meiotic prophase in L2 and by early L3 show 2–4, 16, and 10–16 nuclei, respectively, with staining morphology consistent with pachytene (Figure 8C, unpublished results). To assess S phase, early L3 worms were EdU labeled for 30 min and then stained for HIM-3. At early L3, *gld-1*; *glp-1* and *gld-2*; *glp-1* double mutants contained only germ cells with pachytene morphology, where nuclei were EdU− and HIM-3 positive. By contrast, in *gld-1 prom-1*; *glp-1* and *gld-2 prom-1*; *glp-1* triple mutants, we observed germ cells undergoing active S phase, where nuclei were EdU+ and HIM-3 negative, along with EdU− HIM-3-positive meiotic cells; these results indicate that, while some cells had entered meiosis, a subset of cells failed to enter meiotic prophase and continued mitotic cycling (Figure 7C and Table 4). These observations indicate that the adult overproliferation phenotype in *gld-1 prom-1*; *glp-1* or *gld-2 prom-1*; *glp-1* triple mutants arises due to a failure of germ cells to enter meiotic prophase, although a contribution from return to mitosis of meiotic nuclei at later stages of development is not ruled out.

Early L3 *gld-1 skr-2*; *glp-1* germlines did not show EdU incorporation and all nuclei were HIM-3 positive (Table 4, unpublished results), indicating that adult germline overproliferation in this mutant combination is likely due to a return to mitosis of meiotic cells. *skr-1* and *skr-2* are very similar genes and RNAi of either of these results in an identical

Table 3 Overproliferation severity and epistasis of SCF^{PROM-1} and GLD-1or GLD-2 pathway gene double mutants with *glp-1*

Genotype	Adult overproliferation (%)	n^a	Overproliferation severity in adults[b]
gld-1	100	>100	++
gld-1; glp-1	0	20	–
fog-1 gld-1;glp-1	100	20	+
gld-1 prom-1	100	>100	+++
gld-1 prom-1; glp-1	100	>100	+
gld-2 prom-1	100	>100	++
gld-2 prom-1; glp-1	100	>100	++
prom-1; gld-3	100	90	++
prom-1; gld-3; glp-1	100	45	+
gld-1 skr-2	100	100	++
gld-1 skr-2; glp-1	100	30	+
gld-2 skr-2	28	112	+
gld-2 skr-2; glp-1	Glp[c]	30	–
skr-2; gld-3	91	121	+
skr-2; gld-3; glp-1	100	196	+
gld-4[d]	0	30	–
gld-4 prom-1[e]	100	30	+

[a] Number of gonad arms analyzed.
[b] Overproliferation severity was qualitatively determined based on number of S-phase nuclei. Overproliferation of *gld-1* mutant germline is arbitrarily taken as ++, and gonads from age-matched animals of different genotypes are classified as less severe (+) or more severe (+++) than *gld-1* mutant germlines.
[c] All germ cells entered meiosis but are arrested with a pachytene-like morphology.
[d] Hermaphrodites grown at 25°.
[e] Hermaphrodites grown at 25°.

phenotype (table 7 in Nayak *et al.* 2002). The *skr-1* mutant is superficially wild type, whereas many defects in *skr-1* or *skr-2* RNAi (Nayak *et al.* 2002) are present in *skr-2* single mutants. We reasoned that SKR-1 may function redundantly with SKR-2 during larval development. Thus, we depleted *skr-1* by RNAi in *gld-1 skr-2*; *glp-1* worms. While we did not observe EdU incorporation in GFP (control) RNAi in L3 worm germlines (unpublished results), the triple mutant with *skr-1* RNAi showed EdU+ germ cells (Figure 8C and Table 4). This finding indicates that while SKR-2 is the main component of SCF^{PROM-1} in the young adult, SKR-1 also plays a role in promoting meiotic entry/inhibiting germ cell proliferation during larval development. Taken together, these results indicate that SCF^{PROM-1} acts downstream of GLP-1 Notch signaling to promote meiotic entry/inhibit proliferation.

SCF^{PROM-1} functions in parallel to the GLD-1 and GLD-2 pathways to promote meiotic entry

The results presented thus far are consistent with the model that SCF^{PROM-1} functions in parallel to both the GLD-1 and GLD-2 pathways to promote meiotic entry. However, the results are also consistent with SCF^{PROM-1} acting downstream of both the GLD-1 and GLD-2 pathways. As indicated above, the tumors in double mutants knocking out both the GLD-1 and GLD-2 pathways show residual meiotic entry. We predict that if SCF^{PROM-1} functions in parallel to both the GLD-1 and GLD-2 pathways, then loss of SCF^{PROM-1} function in GLD-1 GLD-2 pathway double mutants should decrease or eliminate the residual meiotic entry.

We first compared germlines from *gld-2*; *nos-3* double mutants with *gld-2 prom-1*; *nos-3* triple mutants for the extent of meiotic entry. NOS-3 functions with GLD-2 to promote GLD-1 accumulation in the germline and the *gld-2*; *nos-3* double mutant germline is tumorous, but there is appreciable meiotic entry in the distal gonad arm (Hansen *et al.* 2004a). We stained young-adult germlines with HIM-3 and calculated a meiotic index as a ratio of the total number of HIM-3-positive nuclei to total nuclei (identified by DAPI staining). The germlines were divided into five regions, as described above (Figure S11B). The meiotic index was calculated separately for each region and compared with respective regions of each genotype. About 50% of cells in regions 2 and 3 of the *gld-2*; *nos-3* double mutant germlines were in meiotic prophase. In contrast, *gld-2 prom-1*; *nos-3* germlines showed a drastic reduction in meiotic index in these two regions: from 49% in the double mutant to 5% in the triple mutant in region 2, and from 56 to 7% in region 3 (Figure S17; unpublished results). Thus, loss of SCF^{PROM-1} significantly enhanced the meiotic entry defect of *gld-2*; *nos-3* double mutants. In addition, the triple mutant germline had an increase in total number of cells compared with the double mutant (unpublished results).

To confirm the above results, we examined meiotic entry in the *gld-2 gld-1* double mutant *vs.* the *gld-2 gld-1 prom-1* triple mutant. Since *gld-2 gld-1* double mutant germlines show very little meiotic entry at an early adult stage (Vought *et al.* 2005; unpublished results), we scored germlines of adult hermaphrodites, 1-day past mid-L4, which show some meiotic entry (Hansen *et al.* 2004b; Maine *et al.* 2004). HIM-3-positive nuclei in the distal germline (regions 1, 2, and 3) was used as a measure of meiotic entry since most germ cells that enter meiosis in the *gld-2 gld-1* double mutant are observed in the distal arm. We observed, on average, 186 meiotic nuclei in the distal arm of the *gld-2 gld-1* double mutant (n = 16;

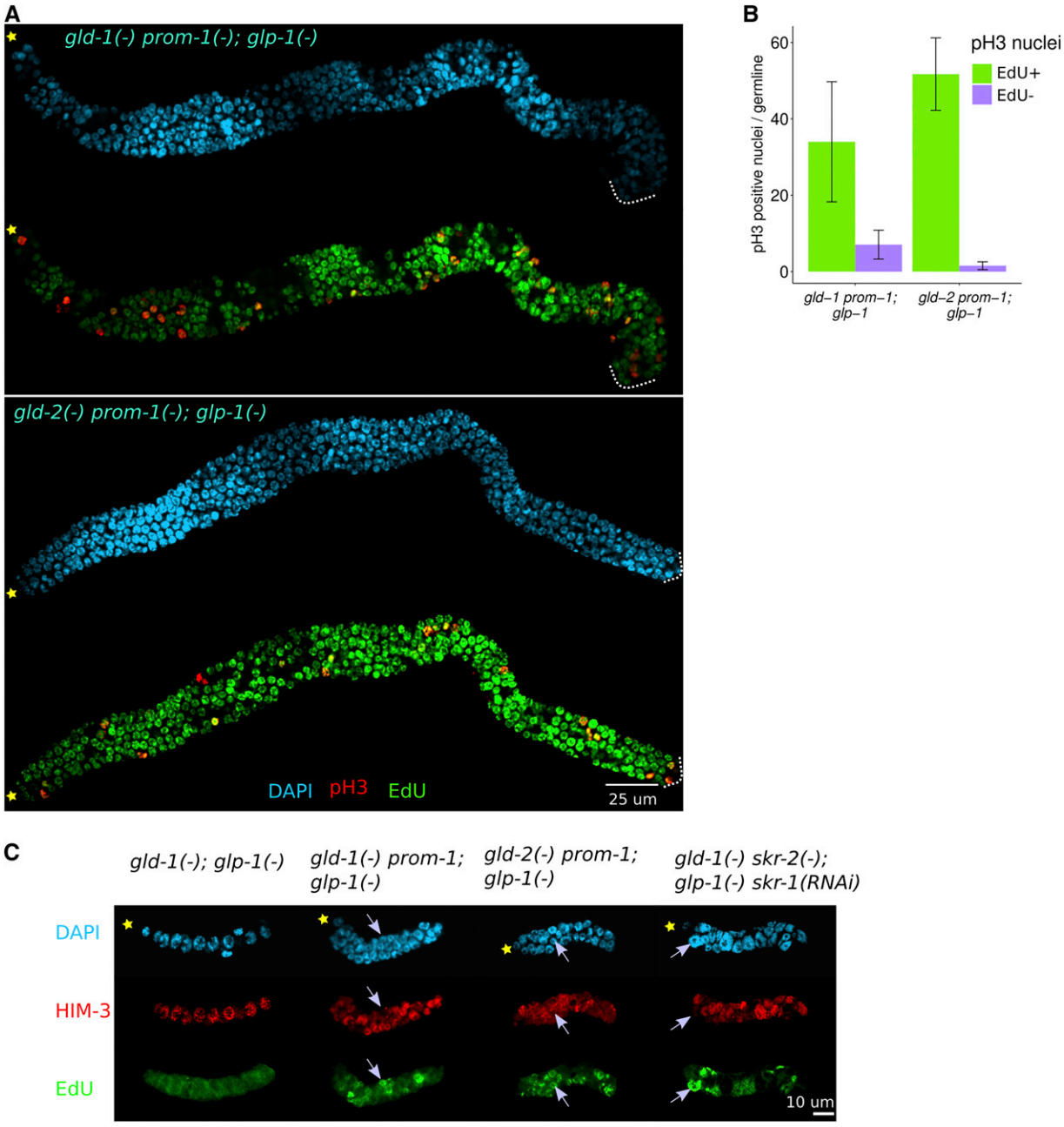

Figure 8 SCF^{PROM-1} meiotic entry defect, with *gld-1* or *gld-2* pathway mutants, is epistatic to *glp-1* null. (A) Images of germlines dissected from young-adult hermaphrodites of the indicated genotype, EdU labeled for 4 hr (green) and costained for pH3 (red) with DAPI (cyan). Dotted white lines indicate proximal end of the germline. (B) Bar graph showing mean number of pH3-positive nuclei per gonad in young hermaphrodite germlines of the indicated genotype (from A). Data are shown for 15 germlines for *gld-1 prom-1*; *glp-1* and 11 germlines for *gld-2 prom-1*; *glp-1*. Error bars indicate mean ± SD. (C) Images of the dissected germlines from L3 hermaphrodites of the indicated genotype. Gonads were EdU-labeled for 30 min and costained for HIM-3 (red) and DAPI (cyan). Gonads were also costained for PGL-1 to distinguish germ cells from somatic cells (data not shown). Note EdU+ nuclei have a strong signal (green), colocalized with chromatin, compared to the background, *e.g.*, in *gld-1*; *glp-1* (left panel) where there are no EdU+ nuclei. *gld-2 prom-1*; *glp-1* L3 germlines showed only cytoplasmic HIM-3 staining, with no colocalization with DNA; the reason for the lack of chromosome loading is unknown. ☆ indicates distal gonadal end. →'s indicate EdU+ nuclei.

Figure 9, A and B); while in *gld-2 gld-1 prom-1* triple mutant distal germlines, the number of meiotic nuclei was reduced drastically to 11 (n = 22; Figure 9, A and B). Taken together, these results support the model that SCF^{PROM-1} functions in parallel with the GLD-1 and GLD-2 pathways to promote meiotic entry.

Ectopic mitotic cell cycle proteins WAPL-1 and CYE-1 contribute to some SCF^{PROM-1} mutant phenotypes

We next asked if ectopic accumulation of cell cycle proteins is responsible for some of the meiotic entry phenotypes observed in SCF^{PROM-1} mutant germlines. In wild-type germlines, REC-8 is present throughout the progenitor zone as nucleoplasmic

Table 4 The *gld-1* or *gld-2* SCF^{PROM-1} double mutant overproliferation defect is due to failure of entry into meiosis

Genotype	Adult overproliferation (%)	L3 EdU+ nuclei[a]
gld-1; *glp-1*	0	Glp
fog-1 gld-1; *glp-1*	ND	Glp
gld-1 prom-1; *glp-1*	100	EdU+
gld-2 prom-1; *glp-1*	100	EdU+
gld-1 skr-2; *glp-1*	100	Glp
gld-2 skr-2; *glp-1*	Glp[b]	Glp
gld-1 skr-2; *glp-1*;*skr-1*(*RNAi*)	ND	EdU+

[a] Young-adult hermaphrodites were assessed for an overproliferation phenotype by EdU incorporation and pH3 staining. Early to mid-L3 hermaphrodites were fed on EdU-labeled bacteria for 30 min and then costained with anti-HIM-3 antibodies as well as anti-PGL-1 antibodies to distinguish germ cells from somatic cells. Glp indicates that all germ cells had entered meiosis. EdU+ indicates germ cells that had undergone EdU incorporation (S phase) during the 30 min pulse, and do not stain for HIM-3.

[b] All germ cells entered meiosis but are arrested with a pachytene-like morphology.

grains, begins to form short axial threads in leptotene–zygotene nuclei, and eventually forms long threads at the pachytene stage (Pasierbek *et al.* 2001). In contrast, at the leptotene–zygotene stage in *prom-1* mutant germlines, only very few small REC-8 threads are formed as well as a few large REC-8 patches/aggregates (Jantsch *et al.* 2007). In mammalian mitosis and *C. elegans* early meiosis, WAPL-1/Wapl has been shown to antagonize cohesion loading onto chromatin (Tedeschi *et al.* 2013; Crawley *et al.* 2016). Since WAPL-1 ectopically accumulates in *prom-1* mutant germlines where REC-8 should be loading on the chromosome axes, we asked if ectopic WAPL-1 is responsible for the REC-8 chromosome-loading defect. We compared REC-8 loading in *prom-1* single mutant germlines with *prom-1*; *wapl-1* double mutant germlines (*Materials and Methods*). Whereas extended early leptotene nuclei of *prom-1* mutant germlines showed very few small REC-8 threads, the *prom-1*; *wapl-1* double mutant germlines showed a significant increase in short REC-8 threads and a loss of the large patches, although a fully wild-type pattern was not observed (Figure 10A). Thus, ectopic WAPL-1, at least in part, is responsible for the REC-8 chromatin-loading defect in *prom-1* mutant germlines.

CYE-1 accumulates throughout the germline of *gld-1 prom-1* double mutants, whereas in wild type it is restricted to the progenitor zone and then late pachytene and developing oocytes. We asked if some of the defects observed in *gld-1 prom-1* germlines could be attributed to ectopic CYE-1. *cye-1* null larvae possess very few germ cells as they are arrested in the mitotic cell cycle and thus cannot be used for our analysis. Therefore, we asked if a reduction of the dose of CYE-1 could suppress or reduce the extended zone of mitotically cycling cells in *gld-1 prom-1* double mutant germlines. For this we compared *gld-1 prom-1* with *cye-1*/+ *gld-1 prom-1* mutant germlines. Young-adult worms were fed EdU-labeled bacteria for 4 hr and costained for the M-phase marker pH3 (Figure 10B). The *cye-1*/+ *gld-1 prom-1* germlines showed a modest, but statistically significant, reduction in the length of the extended zone of mitotically cycling cells compared to *gld-1 prom-1* mutant germlines (Figure 10C). The reduced length of the zone of mitotically cycling cells could be due to either a general effect of dosage reduction of CYE-1 on mitotic cycling, or it could be specific to reduction of ectopic CYE-1. To distinguish between these two possibilities, we compared continuous EdU zone length and pH3-positive nuclei count in *gld-1 vs. cye-1*/+ *gld-1* mutant germlines. If reduction in the extended zone of mitotically cycling cells in *cye-1*/+ *gld-1 prom-1* is due to a general effect of dosage reduction of CYE-1, we would also expect to see a reduction in the length of the EdU zone as well as reduced M-phase cells in the *cye-1*/+ *gld-1* mutant. However, we did not see a significant change in either the number of M-phase cells or in the continuous EdU zone length of *cye-1*/+ *gld-1* as compared to *gld-1* mutant germlines (Figure 10, B and C, and Figure S18). We found similar numbers of M-phase nuclei in region 1 and a slight decrease in region 2 of *cye-1*/+ *gld-1 prom-1* compared to *gld-1 prom-1* mutant germlines, suggesting that cell cycle kinetics largely remain unchanged (Figure 10, B and C, and Figure S18). The reduced length of the extended EdU zone could be responsible for the slight reduction in M-phase cells that we observed in region 2 of the *cye-1*/+ *gld-1 prom-1* mutant. Thus, these findings indicate that ectopic CYE-1, in part, is responsible for the extended zone of mitotically cycling cells of *gld-1 prom-1* mutant germlines. Taken together, the suppression effects with *wapl-1* and *cye-1* indicate that ectopic mitotic cell cycle proteins in SCF^{PROM-1} mutants, and its double mutants with *gld-1* or *gld-2* pathway genes, are in part responsible for the pleiotropy of defects observed.

Discussion

Entry of germ cells into meiotic prophase requires the coordinated downregulation of mitotic cell cycle gene products/activities with the upregulation of gene products/activities that are necessary for meiosis, including those that execute homolog pairing, formation of meiotic chromosome axes, synapsis, and homologous recombination (Hillers *et al.* 2017). We identify the SCF^{PROM-1} ubiquitin-mediated degradation complex as playing an essential role in the downregulation of mitotic cell cycle gene products and promoting pairing of homologous chromosomes. SCF^{PROM-1} functions in parallel with the GLD-1 and GLD-2 pathways to coordinate the many processes required for meiotic entry.

SCF^{PROM-1} downregulates mitotic cell cycle proteins at meiotic entry

Loss of the SCF E3 ubiquitin-ligase complex components *skr-2*, *cul-1*, and *prom-1* results in ectopic accumulation of CYE-1, KNL-2, WAPL-1, and pCDC-6 at meiotic entry. Based on PROM-1–CYE-1 binding in the yeast two-hybrid system, polyubiquitination of CYE-1, and ectopic accumulation of CYE-1 in SCF^{PROM-1} loss of function; CYE-1 appears to be a direct substrate of SCF^{PROM-1} for degradation. This is consistent with the well-known function of the SCF complex in degradation of regulatory proteins to control mitotic cell cycle

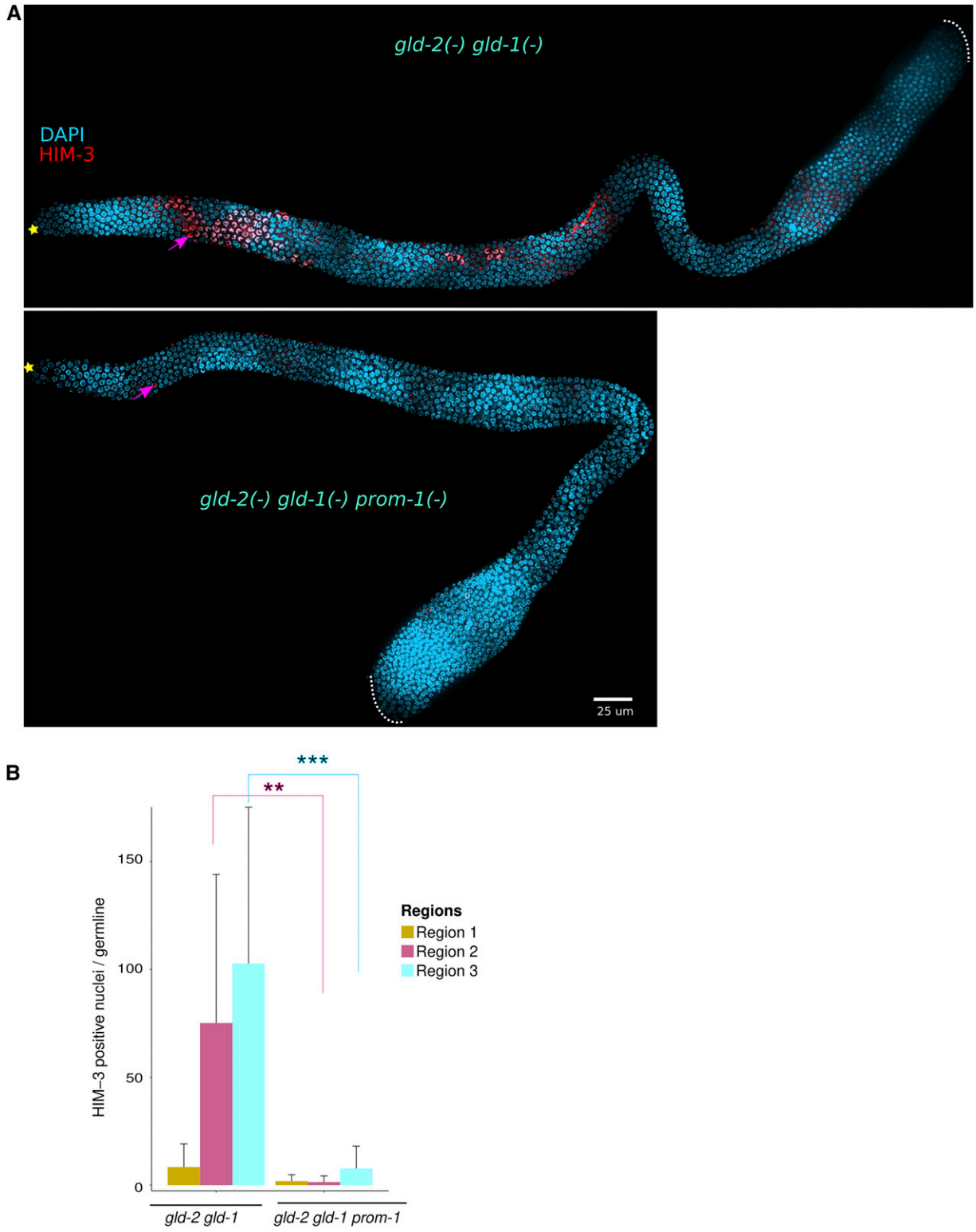

Figure 9 Loss of SCF^{PROM-1} enhances the meiotic entry defect of the *gld-1 gld-2* pathway double mutant. (A) Images of dissected germlines from adult hermaphrodites, 1 day after mid-L4, of the indicated genotype. Gonads were stained for HIM-3 (red) and costained with DAPI (cyan). ☆ indicates distal gonadal end. →'s indicate HIM-3-positive nuclei. Dotted white lines indicate proximal end of the germline. (B) Bar graph showing number of meiotic cells for regions 1–3 (R1, R2, R3), from adult hermaphrodite germlines 1 day after mid-L4, of the indicated genotype. The distal gonad arms, stained for HIM-3 and DAPI (see A above), were divided into the three distal regions as shown in Figure S11B (as essentially no germ cells enter meiosis in regions 4 and 5, they were not analyzed). HIM-3-positive nuclei were counted for each region. Numbers were pooled from each region for individual genotypes, and a mean "total HIM-3-positive nuclei" was calculated. Data are from 16 to 22 germlines for *gld-2 gld-1* and *gld-2 gld-1 prom-1*, respectively. Error bars, SD. *P*-value ≤ 0.001 (**); ≤ 0.0001 (***); > 0.01 non-significant (NS.).

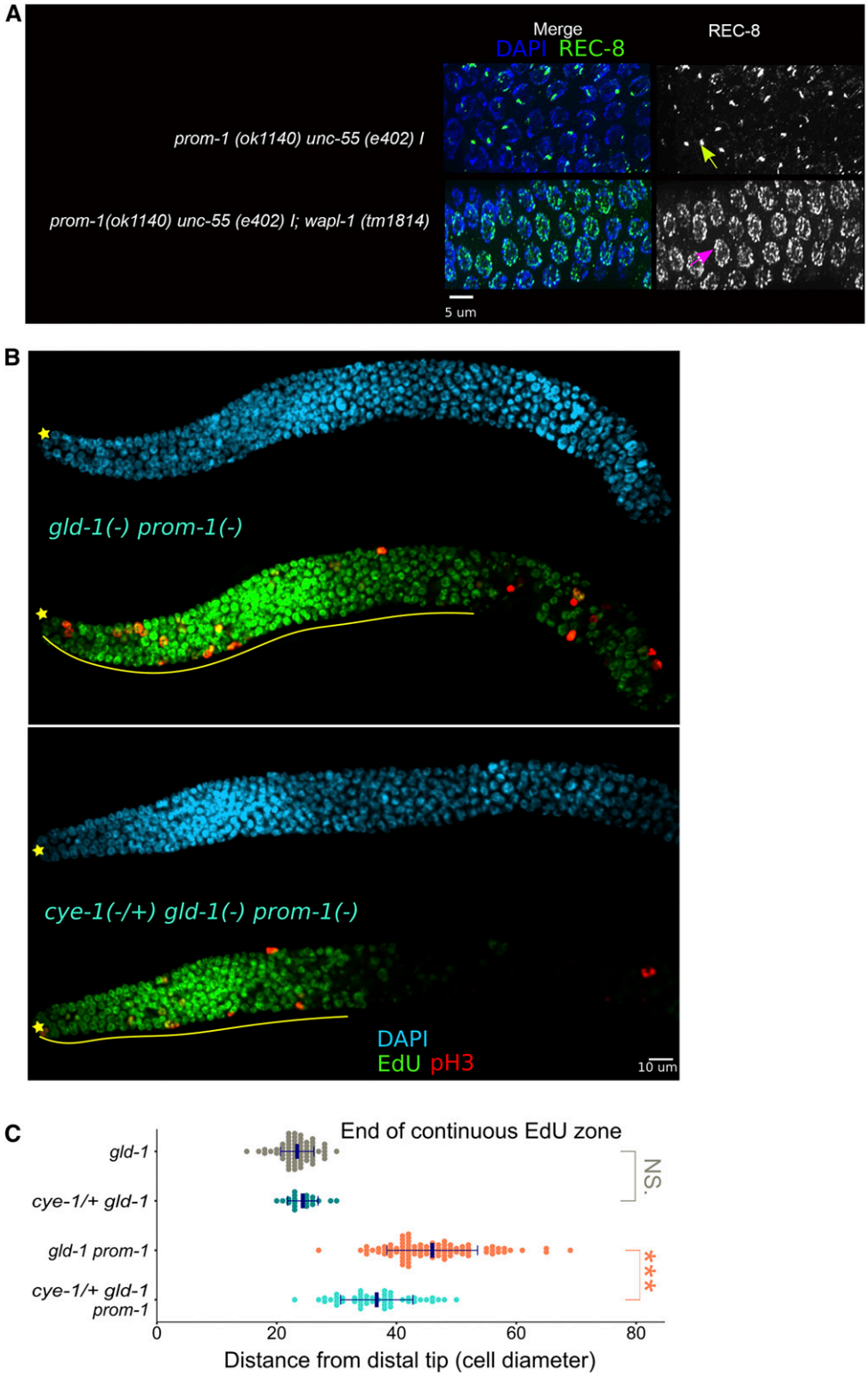

Figure 10 Ectopic WAPL-1 and CYE-1 are responsible for some defects observed in SCF^{PROM-1} mutant germlines. (A) Images of REC-8- and DAPI-stained dissected germlines from adult hermaphrodites, 1 day after mid-L4, of the indicated genotype. The left side of each image corresponds to ~20 cell diameters from the DT. Green → indicates REC-8 aggregate in the *prom-1* single mutant. Pink → indicates REC-8 thread in *prom-1*; *wapl-1* double mutant. Note the significant increase in REC-8 threads in the *prom-1*; *wapl-1* double mutant. (B) Images of distal germline of dissected young adult hermaphrodites of the indicated genotype, following 4-hr EdU labeling (green) and staining for pH3 (red) and DNA (DAPI, cyan). ☆ indicates distal gonadal end. Solid yellow lines indicate continuous EdU zone. (C) Graph showing distance, in cell diameters from the DT, of the continuous EdU zone for young-adult hermaphrodite germlines of the indicated genotypes. Data are plotted as horizontal dot plots with each dot representing length in cell diameter for one gonad. Thick vertical lines represent mean and horizontal lines represent mean ± SD. *P*-value ≤ 0.01 (*); ≤ 0.001 (**); ≤ 0.0001 (***); > 0.01 non-significant (NS.).

transitions (Borg and Dixit 2017). It is not known if KNL-2, WAPL-1, or pCDC-6 are direct substrates of SCF^{PROM-1} or are instead indirect targets. Preliminary results indicate that additional mitotic cell cycle gene products are downregulated by SCF^{PROM-1} (unpublished results). Thus, SCF^{PROM-1} functions to directly downregulate CYE-1 and likely other mitotic cell cycle proteins in the developmental transition to meiotic entry in *C. elegans* (Figure 11A). Although CYE-1, KNL-2, WAPL-1, and pCDC-6 levels remain elevated in SCF^{PROM-1} loss-of-function germlines, eventually they are downregulated (~35–40 cell diameters from the DT). In the case of CYE-1, and possibly others, the more proximal downregulation is due

to translational repression by GLD-1 (Figure S19; Biedermann *et al.* 2009; Fox *et al.* 2011); presumably in the absence of SCF^{PROM-1}, CYE-1 has a long half-life resulting in a delay in observing a reduction in levels due to translational repression. Thus downregulation of CYE-1 in the distal germline is the result of sequential SCF^{PROM-1}-mediated protein degradation in leptotene–zygotene and translational repression mediated by GLD-1 in pachytene (Figure 11B).

SCF^{PROM-1} promotes homologous chromosome pairing

The CHK-2 kinase is a master regulator directing homologous chromosome pairing in *C. elegans* (MacQueen and Villeneuve 2001; Oishi *et al.* 2001; Penkner *et al.* 2009; Stamper *et al.* 2013; Kim *et al.* 2015). Based on the failure of multiple CHK-2-dependent activities to be executed at meiotic entry in SCF^{PROM-1} loss-of-function mutants (appearance of phosphorylated substrates pHIM-8/ZIMs and pSUN-1, DHC-1 nuclear envelope aggregates, and DSB-1 localization to chromatin), we conclude that SCF^{PROM-1} is a positive regulator of CHK-2-dependent pairing. A number of results indicate that SCF^{PROM-1}-mediated downregulation of CYE-1 accumulation, and possibly other mitotic cell cycle proteins, is separate from SCF^{PROM-1} promotion of CHK-2-dependent homolog pairing (Figure 11A). First, CYE-1 levels are downregulated normally at meiotic entry in *chk-2* null germlines, indicating that CHK-2 is not a regulator of CYE-1 levels or SCF^{PROM-1}. Second, CYE-1 levels and CHK-2 activity can be uncoupled, indicating that CYE-1 is not functioning as an inhibitor of CHK-2 or pairing. Third, synthetic overproliferation is not observed in *gld-1*; *chk-2* double mutants (unpublished result), unlike in *gld-1* SCF^{PROM-1} loss-of-function double mutants, indicating that CHK-2 and pairing contributes to only a subset of SCF^{PROM-1} activities. Accordingly, we place downregulation of CYE-1, and possibly other mitotic cell cycle proteins, and promotion of CHK-2-dependent pairing as independent downstream outputs of SCF^{PROM-1}. SCF^{PROM-1} thus coordinates disparate activities important for meiotic development, inhibition of mitotic cell cycling through downregulation of CYE-1 and other mitotic cell cycle proteins, and activation of a meiotic process—pairing.

While SCF^{PROM-1} is a positive regulator of CHK-2, the control mechanism cannot be direct as SCF^{PROM-1} functions to degrade gene products. Instead, we propose that SCF^{PROM-1} degrades a negative regulator (protein X) of CHK-2 (Figure 11A). In the absence of SCF^{PROM-1} activity, negative regulator X remains active at meiotic entry, inhibiting CHK-2, which would result in the absence of pairing. We speculate that negative regulator X inhibits CHK-2 activity in the progenitor zone to prevent activating the homologous chromosome pairing process during mitotic cell cycling, which is likely detrimental to DNA replication and mitotic chromosome segregation. We propose that, at meiotic entry, SCF^{PROM-1} becomes active and degrades negative regulator X, thus activating CHK-2 to initiate pairing. Since the identity of protein X is not known, current data does not exclude the possibility that it may have additional functions such as promoting mitotic cell cycling or stem cell function. As summarized below, SCF^{PROM-1} activity is inhibited by GLP-1 signaling in stem cells/the progenitor zone. Together, these results indicate that SCF^{PROM-1} functions in a pathway to spatially control pairing during germline stem cell differentiation, so that it occurs only at meiotic entry.

We find that at least one of the meiotic phenotypes observed in SCF^{PROM-1} loss of function is due, in part, to ectopic accumulation of a cell cycle protein, the mitotic cohesin chaperon WAPL-1, at meiotic entry. In *prom-1* single mutants, REC-8 loading on to the meiotic chromosome axes is defective, while in *prom-1*; *wapl-1* double mutants the REC-8 loading defect is ameliorated. Presumably, ectopic WAPL-1 at meiotic entry leads to inappropriate removal of REC-8 from the forming meiotic chromosome axes.

SCF^{PROM-1} functions in parallel to the GLD-1 and GLD-2 pathways to promote meiotic entry

Previous studies established that the GLD-1 and GLD-2 pathways function redundantly to promote meiotic entry, acting downstream and inhibited by GLP-1 signaling, which promotes the stem cell fate (Kadyk and Kimble 1998; Eckmann *et al.* 2002; Hansen *et al.* 2004a). We propose that SCF^{PROM-1} is an additional pathway that functions in parallel, redundant with both the GLD-1 and GLD-2 pathways to promote meiotic entry (Figure 11C). This proposal is based on finding that SCF^{PROM-1} loss of function shows a synthetic overproliferation phenotype with both the loss of GLD-1 pathway function (*gld-1* or *nos-3* null mutants) and the loss of GLD-2 pathway function [*gld-2*, *gld-3*, or *gld-4* (25°) null mutants]. Furthermore, the synthetic overproliferation phenotype with loss of GLD-1 or GLD-2 pathway function is epistatic to the premature meiotic entry phenotype of *glp-1* null, indicating that, like the GLD-1 and GLD-2 pathways, promotion of meiotic entry by SCF^{PROM-1} is downstream and inhibited by GLP-1 signaling (Figure 11C). Moreover, we found that loss of SCF^{PROM-1} suppresses the residual meiotic entry that occurs in GLD-1 and GLD-2 pathway null double mutants, indicating that SCF^{PROM-1} acts in parallel to the GLD-1 and GLD-2 pathways, rather than downstream of the combination. Additionally, GLP-1 signaling to promote the stem cell fate, as well as the redundant function of the GLD-1 and GLD-2 pathways to promote meiotic entry, is independent of germ cell sexual fate (Austin and Kimble 1987; Berry *et al.* 1997; Kadyk and Kimble 1998; Eckmann *et al.* 2002; Hansen *et al.* 2004b). Similarly, the redundant function of SCF^{PROM-1} with the GLD-1 pathway and with the GLD-2 pathway to promote meiotic entry is independent of germ cell sexual fate.

The SCF^{PROM-1} meiotic entry pathway also displays a number of differences from the GLD-1 and GLD-2 pathways, which likely reflect their different functions. First, GLD-1 pathway and GLD-2 pathway single mutants enhance the overproliferation phenotype of weak *glp-1* gain-of-function alleles (Hansen *et al.* 2004b), while SCF^{PROM-1} loss of function does not (unpublished result). In the case of *gld-1*, the enhancement is likely because GLD-1 functions in a negative

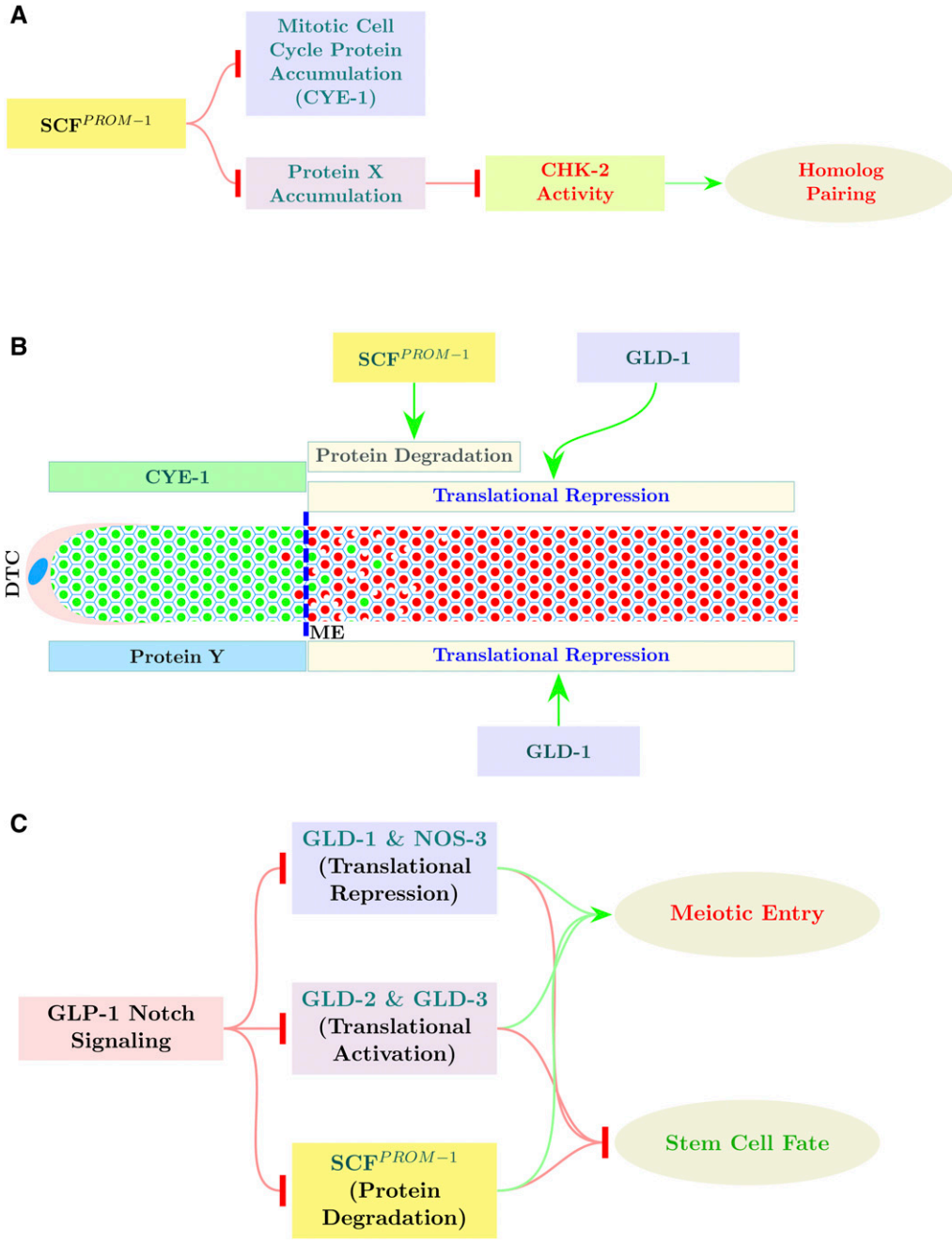

Figure 11 SCF^{PROM-1} function in the control of meiotic entry. (A) Model for SCF^{PROM-1} functioning independently in the downregulation of mitotic cell cycle protein accumulation (CYE-1) and the promotion of homolog pairing through activation of CHK-2, via degradation of a proposed inhibitor of CHK-2, protein X. (B) Model showing downregulation of CYE-1 (green rectangle) levels through dual regulation by SCF^{PROM-1} (proteolysis) and GLD-1 (translational repression); loss of CYE-1 by translational repression is slow, whereas CYE-1 protein degradation is rapid. Protein Y (blue rectangle) is a proposed translational target of GLD-1; in *gld-1*(-) *SCF*$^{PROM-1}$ loss of function, the combination of ectopic protein Y and ectopic mitotic cell cycle proteins (*e.g.*, CYE-1) results in continuous mitotic cell cycling. (C) SCF^{PROM-1} acts in parallel to the GLD-1 pathway and the GLD-2 pathway, downstream of GLP-1 signaling, to promote meiotic entry and inhibit mitotic cell cycling and the stem cell fate. DTC, DT cell.

feedback loop with GLP-1 signaling (Berry *et al.* 1997; Marin and Evans 2003); SCF^{PROM-1} may not function in feedback regulation of GLP-1 signaling. Second, meiotic entry is essentially normal in GLD-1 and GLD-2 pathway single mutants, while in SCF^{PROM-1} mutants there is a failure to downregulate mitotic cell cycle proteins and a failure in meiotic chromosome pairing. Downregulation of mitotic cell cycle proteins and the pairing observed in GLD-1 and GLD-2 pathway single mutants are presumably achieved by the action of SCF^{PROM-1}. Similarly, the absence of ectopic proliferation, notwithstanding the failure to downregulate mitotic cell cycle proteins in SCF^{PROM-1} loss-of-function hermaphrodites, is a consequence of GLD-1 and GLD-2 pathway activity. Third, the GLD-1 and GLD-2 pathways together promote the gametogenic programs, as pathway double mutants show no evidence of spermatogenesis or oogenesis (Kadyk and Kimble 1998; Eckmann *et al.* 2002; Hansen *et al.* 2004b). In contrast, SCF^{PROM-1} *gld-1* double mutant males can make some sperm (Figure S12A) and SCF^{PROM-1} GLD-2 pathway double mutant hermaphrodites can make oocyte like cells (Figure S15). Thus, SCF^{PROM-1} may not have a role in promoting gametogenesis.

In SCF^{PROM-1} loss-of-function hermaphrodites, overproliferation just proximal to the progenitor zone is not observed despite the presence of ectopic mitotic cell cycle proteins. By contrast, in *gld-1* SCF^{PROM-1} loss-of-function double mutants, an extended zone of mitotic cycling cells is found in the

region where ectopic cell cycle proteins are observed. Based on this difference, we propose that GLD-1 must be translationally repressing an mRNA, encoding protein Y, that promotes mitotic cell cycling (Figure 11B). However, the presence of protein Y is not sufficient for mitotic cycling as germ cells stop mitotic cycling at the end of the progenitor zone in *gld-1* null single mutants. Thus, it is the simultaneous presence of ectopic mitotic cell cycle proteins, from loss of SCF^{PROM-1}, and protein Y, from loss of GLD-1, that leads to overproliferation.

Interestingly, in SCF^{PROM-1} single mutant loss-of-function males, unlike mutant hermaphrodites, an extended zone of mitotic cycling cells is observed. In wild type, GLD-1 protein levels are sexually dimorphic, rising ~20-fold at meiotic entry in hermaphrodites, but rising significantly less in males (Jones *et al.* 1996; Lee *et al.* 2007; Brenner and Schedl 2016). Thus, one possibility is that, because of low GLD-1 levels in males, SCF^{PROM-1} loss-of-function males are analogous to *gld-1* SCF^{PROM-1} loss-of-function hermaphrodites, allowing expression of protein Y. This would provide an explanation for suppression of the extended zone of mitotic cycling in *fog-1 prom-1* double mutant males; feminization of the *prom-1* male germline would increase GLD-1 levels, which would more fully repress expression of protein Y.

Spatial control of SCF^{PROM-1} activity

SCF^{PROM-1} appears to be acting at meiotic entry, after completion of meiotic S phase, based on the position where ectopic mitotic cell cycle proteins are observed and failure of pairing occurs in SCF^{PROM-1} loss of function. We argue above that GLD-1 is also acting at meiotic entry to repress the translation of the mRNA for protein Y; when protein Y is inappropriately expressed it promotes mitotic cycling of cells in SCF^{PROM-1} loss of function with ectopic CYE-1. The action of meiotic entry factors after completion of meiotic S phase is consistent with the model that the progenitor zone lacks transit-amplifying cells and that, following loss of GLP-1 signaling, germ cells complete the ongoing mitotic cell cycle and begin meiotic S phase (Fox and Schedl 2015). However, the GLD-1 and GLD-2 pathways appear to also have earlier activities that are important for successful meiotic entry. For example, the level of GLD-1 achieved at ~12–13 cell diameters from the DT in wild-type germlines is correlated with irreversible commitment to meiotic entry and NOS-3, GLD-2, and GLD-3 promote the rise in GLD-1 levels in the proximal progenitor zone (Kadyk and Kimble 1998; Eckmann *et al.* 2002, 2004; Hansen *et al.* 2004a,b; Suh *et al.* 2009; Brenner and Schedl 2016). Further insight will come from uncovering the mechanism by which SCF^{PROM-1} activity is controlled.

Multi-pathway control of meiotic entry and gametogenesis

C. elegans employs three post-transcriptional pathways to achieve meiotic entry: SCF^{PROM-1} substrate-specific protein degradation, GLD-1-mediated translational repression, and GLD-2-mediated translational activation. For SCF^{PROM-1}, we have identified some direct and indirect targets: mitotic cell cycle proteins (CYE-1, KNL-2, WAPL-1, and pCDC-6) and protein X, a proposed inhibitor of homolog pairing. For GLD-1 and GLD-2, direct meiotic entry targets remain to be identified.

In mouse there also appear to be multiple pathways that act together to promote meiotic entry and gametogenesis. Retinoic acid (RA) is the temporospatial inducer of meiotic entry and gametogenesis in mice (Griswold 2016). RA activates the transcription of *Stra8*, a putative transcription factor that promotes multiple aspects of meiotic entry in mouse spermatogenesis and oogenesis, including expression of recombinase *Dmc1* for example (Anderson *et al.* 2008). RA, independent of *Stra8*, promotes the expression of *Rec8*, as well as other early meiotic genes (Koubova *et al.* 2014; Soh *et al.* 2015). Interestingly, *Meioc*, which functions at least partially independently of *Stra8*, appears to have an analogous function to SCF^{PROM-1} and GLD-1: inhibition of mitotic cell cycle protein expression during early meiotic prophase (Abby *et al.* 2016; Soh *et al.* 2017). In addition to the *Stra8* and the *Stra8*-independent meiotic pathways, there is a separate pathway for gametogenesis (Dokshin *et al.* 2013).

In *C. elegans*, in addition to the three meiotic entry pathways (Figure 11C), as germ cells move away from GLP-1 signaling, relief of translational repression by FBF promotes the rise in GLD-1 accumulation and the expression of meiotic chromosome axes proteins (HIM-3) and synaptonemal complex proteins (SYP-1) (Crittenden *et al.* 2002; Kershner and Kimble 2010; Merritt and Seydoux 2010). Are there yet other pathways that promote meiotic entry in *C. elegans*? The finding that there are still some germ cells that enter meiosis in the *gld-2 gld-1 prom-1* null triple mutant is consistent with the possibility that there are additional activities that promote meiotic entry in *C. elegans*. Furthermore, we know little about transcriptional control of meiotic and gametogenic gene products.

Acknowledgments

We thank our colleagues in the germline and meiosis fields for antibodies, helpful discussions, and software: Swathi Arur, Rafal Ciosk, Arshad Desai, Abby Dernburg, Yumi Kim, Judith Kimble, Edward Kipreos, Josef Loidl, Barbara Meyer, Hannah Seidel, Aaron Severson, Anne Villeneuve, and Monique Zetka. We thank Carrie Shemanko for use of tissue culture facilities. We thank WormBase, funded by the National Human Genome Research Institute; the *Caenorhabditis* Genetics Center, funded by National Institutes of Health Office of Research Infrastructure Programs (P40 OD-010440); and Shohei Mitani and the Japanese National Bioresource Project for strains. This work is supported by National Institutes of Health R01 GM-100756 to T.S., from the Natural Sciences and Engineering Research Council of Canada (NSERC) to D.H., and the Austrian Science Fund (SFB F3415-B19) to V.J.

Literature Cited

Abby, E., S. Tourpin, J. Ribeiro, K. Daniel, S. Messiaen *et al.*, 2016 Implementation of meiosis prophase I programme requires a conserved retinoid-independent stabilizer of meiotic transcripts. Nat. Commun. 7: 10324. https://doi.org/10.1038/ncomms10324

Anderson, E. L., A. E. Baltus, H. L. Roepers-Gajadien, T. J. Hassold, D. G. de Rooij *et al.*, 2008 Stra8 and its inducer, retinoic acid, regulate meiotic initiation in both spermatogenesis and oogenesis in mice. Proc. Natl. Acad. Sci. USA 105: 14976–14980. https://doi.org/10.1073/pnas.0807297105

Austin, J., and J. Kimble, 1987 glp-1 Is required in the germ line for regulation of the decision between mitosis and meiosis in C. elegans. Cell 51: 589–599. https://doi.org/10.1016/0092-8674(87)90128-0

Barton, M. K., and J. Kimble, 1990 fog-1, a regulatory gene required for specification of spermatogenesis in the germ line of Caenorhabditis elegans. Genetics 125: 29–139.

Barton, M. K., T. B. Schedl, and J. Kimble, 1987 Gain-of-function mutations of fem-3, a sex-determination gene in Caenorhabditis elegans. Genetics 115: 107–119.

Berry, L. W., B. Westlund, and T. Schedl, 1997 Germ-line tumor formation caused by activation of glp-1, a Caenorhabditis elegans member of the Notch family of receptors. Development 124: 925–936.

Biedermann, B., J. Wright, M. Senften, I. Kalchhauser, G. Sarathy *et al.*, 2009 Translational repression of cyclin E prevents precocious mitosis and embryonic gene activation during C. elegans meiosis. Dev. Cell 17: 355–364. https://doi.org/10.1016/j.devcel.2009.08.003

Borg, N. A., and V. M. Dixit, 2017 Ubiquitin in cell-cycle regulation and dysregulation in cancer. Annual Review of Cancer Biology 1: 59–77. https://doi.org/10.1146/annurev-cancerbio-040716-075607

Brenner, J. L., and T. Schedl, 2016 Germline stem cell differentiation entails regional control of cell fate regulator GLD-1 in Caenorhabditis elegans. Genetics 202: 1085–1103. https://doi.org/10.1534/genetics.115.185678

Brodigan, T. M., J. i. Liu, M. Park, E. T. Kipreos, and M. Krause, 2003 Cyclin E expression during development in Caenorhabditis elegans. Dev. Biol. 254: 102–115. https://doi.org/10.1016/S0012-1606(02)00032-5

Crawley, O., C. Barroso, S. Testori, N. Ferrandiz, N. Silva *et al.*, 2016 Cohesin-interacting protein WAPL-1 regulates meiotic chromosome structure and cohesion by antagonizing specific cohesin complexes. eLife 5: e10851. https://doi.org/10.7554/eLife.10851

Crittenden, S. L., D. S. Bernstein, J. L. Bachorik, B. E. Thompson, M. Gallegos *et al.*, 2002 A conserved RNA-binding protein controls germline stem cells in Caenorhabditis elegans. Nature 417: 660–663. https://doi.org/10.1038/nature754

Dernburg, A. F., K. Mcdonald, G. Moulder, R. Barstead, M. Dresser *et al.*, 1998 Meiotic recombination in C. elegans initiates by a conserved mechanism and is dispensable for homologous chromosome synapsis. Cell 94: 387–398. https://doi.org/10.1016/S0092-8674(00)81481-6

Dokshin, G. A., A. E. Baltus, J. J. Eppig, and D. C. Page, 2013 Oocyte differentiation is genetically dissociable from meiosis in mice. Nat. Genet. 45: 877–883. https://doi.org/10.1038/ng.2672

Eckmann, C. R., B. Kraemer, M. Wickens, J. Kimble, S. Fields *et al.*, 2002 GLD-3, a bicaudal-C homolog that inhibits FBF to control germline sex determination in C. elegans. Dev. Cell 3: 697–710. https://doi.org/10.1016/S1534-5807(02)00322-2

Eckmann, C. R., S. L. Crittenden, N. Suh, and J. Kimble, 2004 GLD-3 and control of the mitosis/meiosis decision in the germline of Caenorhabditis elegans. Genetics 168: 147–160. https://doi.org/10.1534/genetics.104.029264

Fay, D. S., 2013 Classical genetic methods (December 30, 2013), *WormBook*, ed. The *C. elegans* Research Community WormBook, http://www.wormbook.org. https://doi.org/10.1895/wormbook.1.165.1

Fox, P. M., and T. Schedl, 2015 Analysis of germline stem cell differentiation following loss of GLP-1 notch activity in Caenorhabditis elegans. Genetics 201: 167–184. https://doi.org/10.1534/genetics.115.178061

Fox, P. M., V. E. Vought, M. Hanazawa, M.-H. Lee, E. M. Maine *et al.*, 2011 Cyclin E and CDK-2 regulate proliferative cell fate and cell cycle progression in the C. elegans germline. Development 138: 2223–2234. https://doi.org/10.1242/dev.059535

Francis, R., M. K. Barton, J. Kimble, and T. Schedl, 1995a gld-1, a tumor suppressor gene required for oocyte development in Caenorhabditis elegans. Genetics 139: 579–606.

Francis, R., E. Maine, and T. Schedl, 1995b Analysis of the multiple roles of gld-1 in germline development: interactions with the sex determination cascade and the glp-1 signaling pathway. Genetics 139: 607–630.

Gandhi, R., P. J. Gillespie, T. Hirano, N. Mahmood, M. Mumby *et al.*, 2006 Human Wapl is a cohesin-binding protein that promotes sister-chromatid resolution in mitotic prophase. Curr. Biol. 16: 2406–2417. https://doi.org/10.1016/j.cub.2006.10.061

Green, R. A., H.-L. Kao, A. Audhya, S. Arur, J. R. Mayers *et al.*, 2011 A high-resolution C. elegans essential gene network based on phenotypic profiling of a complex tissue. Cell 145: 470–482. https://doi.org/10.1016/j.cell.2011.03.037

Griswold, M. D., 2016 Spermatogenesis: the commitment to meiosis. Physiol. Rev. 96: 1–17. https://doi.org/10.1152/physrev.00013.2015

Hansen, D., and T. Schedl, 2013 Stem cell proliferation versus meiotic fate decision in Caenorhabditis elegans. Adv. Exp. Med. Biol. 757: 71–99. https://doi.org/10.1007/978-1-4614-4015-4_4

Hansen, D., E. J. A. Hubbard, and T. Schedl, 2004a Multi-pathway control of the proliferation *vs.* meiotic development decision in the Caenorhabditis elegans germline. Dev. Biol. 268: 342–357. https://doi.org/10.1016/j.ydbio.2003.12.023

Hansen, D., L. Wilson-Berry, T. Dang, and T. Schedl, 2004b Control of the proliferation *vs.* meiotic development decision in the C. elegans germline through regulation of GLD-1 protein accumulation. Development 131: 93–104. https://doi.org/10.1242/dev.00916

Hillers, K. J., V. Jantsch, E. Martinez-Perez, and J. L. Yanowitz, 2017 Meiosis (May 4, 2017), *WormBook*, ed. The *C. elegans* Research Community, WormBook, 10.1895/wormbook.1.178.1, http://www.wormbook.org.

Hong, Y., R. Roy, and V. Ambros, 1998 Developmental regulation of a cyclin-dependent kinase inhibitor controls postembryonic cell cycle progression in Caenorhabditis elegans. Development 125: 3585.

Hruz, T., O. Laule, G. Szabo, F. Wessendorp, S. Bleuler *et al.*, 2008 Genevestigator v3: a reference expression database for the meta-analysis of transcriptomes. Adv. Bioinforma. 2008: 420747. https://doi.org/10.1155/2008/420747

Hubbard, E. J. A., 2007 The *C. elegans* germ line: a model for stem cell biology. Dev. Dyn. 236: 3343–3357. https://doi.org/10.1002/dvdy.21335

Jantsch, V., L. Tang, P. Pasierbek, A. Penkner, S. Nayak *et al.*, 2007 Caenorhabditis elegans prom-1 is required for meiotic prophase progression and homologous chromosome pairing. Mol. Biol. Cell 18: 4911–4920. https://doi.org/10.1091/mbc.e07-03-0243

Jaramillo-Lambert, A., M. Ellefson, A. M. Villeneuve, and J. A. Engebrecht, 2007 Differential timing of S phases, X chromosome

replication, and meiotic prophase in the C. elegans germ line. Dev. Biol. 308: 206–221. https://doi.org/10.1016/j.ydbio.2007.05.019

Jones, A. R., and T. Schedl, 1995 Mutations in gld-1, a female germ cell-specific tumor suppressor gene in Caenorhabditis elegans, affect a conserved domain also found in Src-associated protein Sam68. Genes Dev. 9: 1491–1504. https://doi.org/10.1101/gad.9.12.1491

Jones, A. R., R. Francis, and T. Schedl, 1996 GLD-1, a cytoplasmic protein essential for oocyte differentiation, shows stage- and sex-specific expression during Caenorhabditis elegans germline development. Dev. Biol. 180: 165–183. https://doi.org/10.1006/dbio.1996.0293

Kadyk, L. C., and J. Kimble, 1998 Genetic regulation of entry into meiosis in Caenorhabditis elegans. Development 125: 1803–1813.

Kalchhauser, I., B. M. Farley, S. Pauli, S. P. Ryder, and R. Ciosk, 2011 FBF represses the Cip/Kip cell-cycle inhibitor CKI-2 to promote self-renewal of germline stem cells in C. elegans. EMBO J. 30: 3823–3829. https://doi.org/10.1038/emboj.2011.263

Kerins, J. A., M. Hanazawa, M. Dorsett, and T. Schedl, 2010 PRP-17 and the pre-mRNA splicing pathway are preferentially required for the proliferation *vs.* meiotic development decision and germline sex determination in Caenorhabditis elegans. Dev. Dyn. 239: 1555–1572. https://doi.org/10.1002/dvdy.22274

Kershner, A., S. L. Crittenden, K. Friend, E. B. Sorensen, D. F. Porter *et al.*, 2013 Germline Stem Cells and Their Regulation in the Nematode Caenorhabditis elegans. *Adv Exp Med Biol.* 786: 29–46 https://doi.org/10.1007/978-94-007-6621-1_3

Kershner, A. M., and J. Kimble, 2010 Genome-wide analysis of mRNA targets for Caenorhabditis elegans FBF, a conserved stem cell regulator. Proc. Natl. Acad. Sci. USA 107: 3936–3941. https://doi.org/10.1073/pnas.1000495107

Kim, Y., and E. T. Kipreos, 2007 The Caenorhabditis elegans replication licensing factor CDT-1 is targeted for degradation by the CUL-4/DDB-1 complex. Mol. Cell. Biol. 27: 1394–1406. https://doi.org/10.1128/MCB.00736-06

Kim, Y., N. Kostow, and A. F. Dernburg, 2015 The chromosome axis mediates feedback control of CHK-2 to ensure crossover formation in C. elegans. Dev. Cell 35: 247–261. https://doi.org/10.1016/j.devcel.2015.09.021

Kimble, J., and J. White, 1981 On the control of germ cell development in Caenorhabditis elegans. Dev. Biol. 81: 208–219. https://doi.org/10.1016/0012-1606(81)90284-0

Kipreos, E. T., L. E. Lander, J. P. Wing, W. W. He, and E. M. Hedgecock, 1996 cul-1 is required for cell cycle exit in C. elegans and identifies a novel gene family. Cell 85: 829–839. https://doi.org/10.1016/S0092-8674(00)81267-2

Kosinski, M., K. McDonald, J. Schwartz, I. Yamamoto, and D. Greenstein, 2005 C. elegans sperm bud vesicles to deliver a meiotic maturation signal to distant oocytes. Development 132: 3357–3369. https://doi.org/10.1242/dev.01916

Koubova, J., Y.-C. Hu, T. Bhattacharyya, Y. Q. S. Soh, M. E. Gill *et al.*, 2014 Retinoic acid activates two pathways required for meiosis in mice. PLoS Genet. 10: e1004541. https://doi.org/10.1371/journal.pgen.1004541

Kueng, S., B. Hegemann, B. H. Peters, J. J. Lipp, A. Schleiffer *et al.*, 2006 Wapl controls the dynamic association of cohesin with chromatin. Cell 127: 955–967. https://doi.org/10.1016/j.cell.2006.09.040

Lee, M. H., and T. Schedl, 2010 C. elegans STAR proteins, GLD-1 and ASD-2, regulate specific RNA targets to control development. Adv. Exp. Med. Biol. 693: 106–122. https://doi.org/10.1007/978-1-4419-7005-3_8

Lee, M. H., M. Ohmachi, S. Arur, S. Nayak, R. Francis *et al.*, 2007 Multiple functions and dynamic activation of MPK-1 extracellular signal-regulated kinase signaling in Caenorhabditis elegans germline development. Genetics 177: 2039–2062. https://doi.org/10.1534/genetics.107.081356

Liu, J., T. R. Ben-shahar, D. Riemer, M. Treinin, K. Weber *et al.*, 2000 Essential roles for Caenorhabditis elegans lamin gene in nuclear organization, cell cycle progression, and spatial organization of nuclear pore complexes. Mol. Biol. Cell 11: 3937–3947. https://doi.org/10.1091/mbc.11.11.3937

MacQueen, A. J., and A. M. Villeneuve, 2001 Nuclear reorganization and homologous chromosome pairing during meiotic prophase require C. elegans chk-2. Genes Dev. 15: 1674–1687. https://doi.org/10.1101/gad.902601

Maddox, P. S., F. Hyndman, J. Monen, K. Oegema, and A. Desai, 2007 Functional genomics identifies a Myb domain-containing protein family required for assembly of CENP-A chromatin. J. Cell Biol. 176: 757–763. https://doi.org/10.1083/jcb.200701065

Mailand, N., and J. F. Diffley, 2005 CDKs promote DNA replication origin licensing in human cells by protecting Cdc6 from APC/C-dependent proteolysis. Cell 122: 915–926. https://doi.org/10.1016/j.cell.2005.08.013

Maine, E. M., D. Hansen, D. Springer, and V. E. Vought, 2004 Caenorhabditis elegans atx-2 promotes germline proliferation and the oocyte fate. Genetics 168: 817–830. https://doi.org/10.1534/genetics.104.029355

Mantina, P., L. MacDonald, A. Kulaga, L. Zhao, and D. Hansen, 2009 A mutation in teg-4, which encodes a protein homologous to the SAP130 pre-mRNA splicing factor, disrupts the balance between proliferation and differentiation in the C. elegans germ line. Mech. Dev. 126: 417–429. https://doi.org/10.1016/j.mod.2009.01.006

Marin, V. A., and T. C. Evans, 2003 Translational repression of a C. elegans Notch mRNA by the STAR/KH domain protein GLD-1. Development 130: 2623–2632. https://doi.org/10.1242/dev.00486

Marré, J., E. C. Traver, and A. M. Jose, 2016 Extracellular RNA is transported from one generation to the next in Caenorhabditis elegans. Proc. Natl. Acad. Sci. USA 113: 12496–12501. https://doi.org/10.1073/pnas.1608959113

Martinez-Perez, E., and A. M. Villeneuve, 2005 HTP-1-dependent constraints coordinate homolog pairing and synapsis and promote chiasma formation during C. elegans meiosis. Genes Dev. 19: 2727–2743. https://doi.org/10.1101/gad.1338505

Merritt, C., and G. Seydoux, 2010 The Puf RNA-binding proteins FBF-1 and FBF-2 inhibit the expression of synaptonemal complex proteins in germline stem cells. Development 137: 1787–1798. https://doi.org/10.1242/dev.050799

Millonigg, S., R. Minasaki, M. Nousch, J. Novak, and C. R. Eckmann, 2014 GLD-4-Mediated translational activation regulates the size of the proliferative germ cell pool in the adult C. elegans germ line. PLoS Genet. 10: e1004647 [corrigenda: PLoS Genet. 12: e1005862 (2016)]. https://doi.org/10.1371/journal.pgen.1004647

Mlynarczyk-Evans, S., and A. M. Villeneuve, 2017 Time-course analysis of early meiotic prophase events informs mechanisms of homolog pairing and synapsis in caenorhabditis elegans. Genetics 207: 103–114. https://doi.org/10.1534/genetics.117.204172

Nayak, S., F. E. Santiago, H. Jin, D. Lin, T. Schedl *et al.*, 2002 The Caenorhabditis elegans Skp1-related gene family: diverse functions in cell proliferation, morphogenesis, and meiosis. Curr. Biol. 12: 277–287. https://doi.org/10.1016/S0960-9822(02)00682-6

Oishi, I., K. Iwai, Y. Kagohashi, H. Fujimoto, K.-I. Kariya *et al.*, 2001 Critical role of Caenorhabditis elegans homologs of Cds1 (Chk2)-related kinases in meiotic recombination. Mol. Cell Biol. 21: 1329–1335.

Pasierbek, P., M. Jantsch, M. Melcher, A. Schleiffer, D. Schweizer *et al.*, 2001 A Caenorhabditis elegans cohesion protein with functions in meiotic chromosome pairing and disjunction. Genes Dev. 15: 1349–1360. https://doi.org/10.1101/gad.192701

Penengo, L., M. Mapelli, A. G. Murachelli, S. Confalonieri, L. Magri *et al.*, 2006 Crystal structure of the ubiquitin binding domains of Rabex-5 reveals two modes of interaction with ubiquitin. Cell 124: 1183–1195. https://doi.org/10.1016/j.cell.2006.02.020

Penkner, A. M., A. Fridkin, J. Gloggnitzer, A. Baudrimont, T. Machacek *et al.*, 2009 Meiotic chromosome homology search involves modifications of the nuclear envelope protein matefin/SUN-1. Cell 139: 920–933. https://doi.org/10.1016/j.cell.2009.10.045

Phillips, C. M., C. Wong, N. Bhalla, P. M. Carlton, P. Weiser *et al.*, 2005 HIM-8 binds to the X chromosome pairing center and mediates chromosome-specific meiotic synapsis. Cell 123: 1051–1063. https://doi.org/10.1016/j.cell.2005.09.035

Polanowska, J., J. S. Martin, R. Fisher, T. Scopa, I. Rae *et al.*, 2004 Tandem immunoaffinity purification of protein complexes from Caenorhabditis elegans. Biotechniques 36: 778–780, 782. https://doi.org/10.2144/04365BM05

Preibisch, S., S. Saalfeld, and P. Tomancak, 2009 Globally optimal stitching of tiled 3D microscopic image acquisitions. Bioinformatics 25: 1463–1465. https://doi.org/10.1093/bioinformatics/btp184

Priti, A., and K. Subramaniam, 2015 PUF-8 functions redundantly with GLD-1 to promote the meiotic progression of spermatocytes in Caenorhabditis elegans. G3 (Bethesda) 5: 1675–1684. https://doi.org/10.1534/g3.115.019521

Salic, A., and T. J. Mitchison, 2008 A chemical method for fast and sensitive detection of DNA synthesis in vivo. Proc. Natl. Acad. Sci. USA 105: 2415–2420. https://doi.org/10.1073/pnas.0712168105

Sato, A., B. Isaac, C. M. Phillips, R. Rillo, P. M. Carlton *et al.*, 2009 Cytoskeletal forces span the nuclear envelope to coordinate meiotic chromosome pairing and synapsis. Cell 139: 907–919. https://doi.org/10.1016/j.cell.2009.10.039

Schindelin, J., I. Arganda-Carreras, E. Frise, V. Kaynig, M. Longair *et al.*, 2012 Fiji: an open-source platform for biological-image analysis. Nat. Methods 9: 676–682. https://doi.org/10.1038/nmeth.2019

Seidel, H. S., and J. Kimble, 2015 Cell-cycle quiescence maintains Caenorhabditis elegans germline stem cells independent of GLP-1/Notch. eLife 4: e100832. https://doi.org/10.7554/eLife.10832

Severson, A. F., and B. J. Meyer, 2014 Divergent kleisin subunits of cohesin specify mechanisms to tether and release meiotic chromosomes. eLife 3: e03467. https://doi.org/10.7554/eLife.03467

Sherr, C. J., and J. M. Roberts, 1999 CDK inhibitors: positive and negative regulators of G1-phase progression. Genes Dev. 13: 1501–1512. https://doi.org/10.1101/gad.13.12.1501

Shin, H., K. A. Haupt, A. M. Kershner, P. Kroll-Conner, M. Wickens *et al.*, 2017 SYGL-1 and LST-1 link niche signaling to PUF RNA repression for stem cell maintenance in Caenorhabditis elegans. PLoS Genet. 13: e1007121. https://doi.org/10.1371/journal.pgen.1007121

Soh, Y. Q., J. P. Junker, M. E. Gill, J. L. Mueller, A. van Oudenaarden *et al.*, 2015 A gene regulatory program for meiotic prophase in the fetal ovary. PLoS Genet. 11: e1005531. https://doi.org/10.1371/journal.pgen.1005531

Soh, Y. Q., M. M. Mikedis, M. Kojima, A. K. Godfrey, D. G. de Rooij *et al.*, 2017 Meioc maintains an extended meiotic prophase I in mice. PLoS Genet. 13: e1006704. https://doi.org/10.1371/journal.pgen.1006704

Stamper, E. L., S. E. Rodenbusch, S. Rosu, J. Ahringer, A. M. Villeneuve *et al.*, 2013 Identification of DSB-1, a protein required for initiation of meiotic recombination in Caenorhabditis elegans, illuminates a crossover assurance checkpoint. PLoS Genet. 9: e1003679. https://doi.org/10.1371/journal.pgen

Subramaniam, K., and G. Seydoux, 2003 Dedifferentiation of primary spermatocytes into germ cell tumors in C. elegans lacking the pumilio-like protein PUF-8. Curr. Biol. 13: 134–139. https://doi.org/10.1016/S0960-9822(03)00005-8

Suh, N., S. L. Crittenden, A. Goldstrohm, B. Hook, B. Thompson *et al.*, 2009 FBF and its dual control of gld-1 expression in the Caenorhabditis elegans germline. Genetics 181: 1249–1260. https://doi.org/10.1534/genetics.108.099440

Tang, L., T. Machacek, Y. M. Mamnun, A. Penkner, J. Gloggnitzer *et al.*, 2010 Mutations in Caenorhabditis elegans him-19 show meiotic defects that worsen with age. Mol. Biol. Cell 21: 885–896. https://doi.org/10.1091/mbc.e09-09-0811

Tedeschi, A., G. Wutz, S. Huet, M. Jaritz, A. Wuensche *et al.*, 2013 Wapl is an essential regulator of chromatin structure and chromosome segregation. Nature 501: 564–568. https://doi.org/10.1038/nature12471

Vought, V. E., M. Ohmachi, M.-H. Lee, and E. M. Maine, 2005 EGO-1, a putative RNA-directed RNA polymerase, promotes germline proliferation in parallel with GLP-1/notch signaling and regulates the spatial organization of nuclear pore complexes and germline P granules in Caenorhabditis elegans. Genetics 170: 1121–1132. https://doi.org/10.1534/genetics.105.042135

Wang, L., C. R. Eckmann, L. C. Kadyk, M. Wickens, and J. Kimble, 2002 A regulatory cytoplasmic poly(A) polymerase in Caenorhabditis elegans. Nature 419: 312–316. https://doi.org/10.1038/nature01039

Zetka, M. C., I. Kawasaki, S. Strome, and F. Mü Ller, 1999 Synapsis and chiasma formation in Caenorhabditis elegans require HIM-3, a meiotic chromosome core component that functions in chromosome segregation. Genes Dev. 13: 2258–2270. https://doi.org/10.1101/gad.13.17.2258

Zickler, D., and N. Kleckner, 1998 The leptotene-zygotene transition of meiosis. Annu. Rev. Genet. 32: 619–697. https://doi.org/10.1146/annurev.genet.32.1.619

Communicating editor: D. Greenstein